https://doi.org/10.1016/j.scitotenv.2018.08.219

Characteristics of Atmospheric $PM_{2.5}$ Composition during the Implementation of Stringent Pollution Control Measures in Shanghai for the 2016 G20 Summit

Haiwei Li[a], Dongfang Wang[b], Long Cui[a], Yuan Gao[c], Juntao Huo[b], Xinning Wang[b], Zhuozhi Zhang[a], Yan Tan[a], Yu Huang[d], Junji Cao[d], Judith C. Chow[e], Shun-cheng Lee[a]*, Qingyan Fu[b]*

[a]*Department of Civil and Environmental Engineering, The Hong Kong Polytechnic University, Hung Hom, Hong Kong*

[b]*Shanghai Environmental Monitoring Center, Shanghai, China*

[c]*Chu Hai College of Higher Education, Tuen Mun, Hong Kong*

[d]*Key Laboratory of Aerosol Chemistry and Physics, Institute of Earth Environment, Chinese Academy of Sciences, Xi'an 710061, China*

[e]*Division of Atmospheric Sciences, Desert Research Institute, Reno, Nevada, USA*

Correspondence authors:

Prof. Shun-cheng Lee, E-mail: ceslee@polyu.edu.hk

Dr. Qingyan Fu, E-mail: qingyanf@semc.gov.cn

*Graphical Abstract

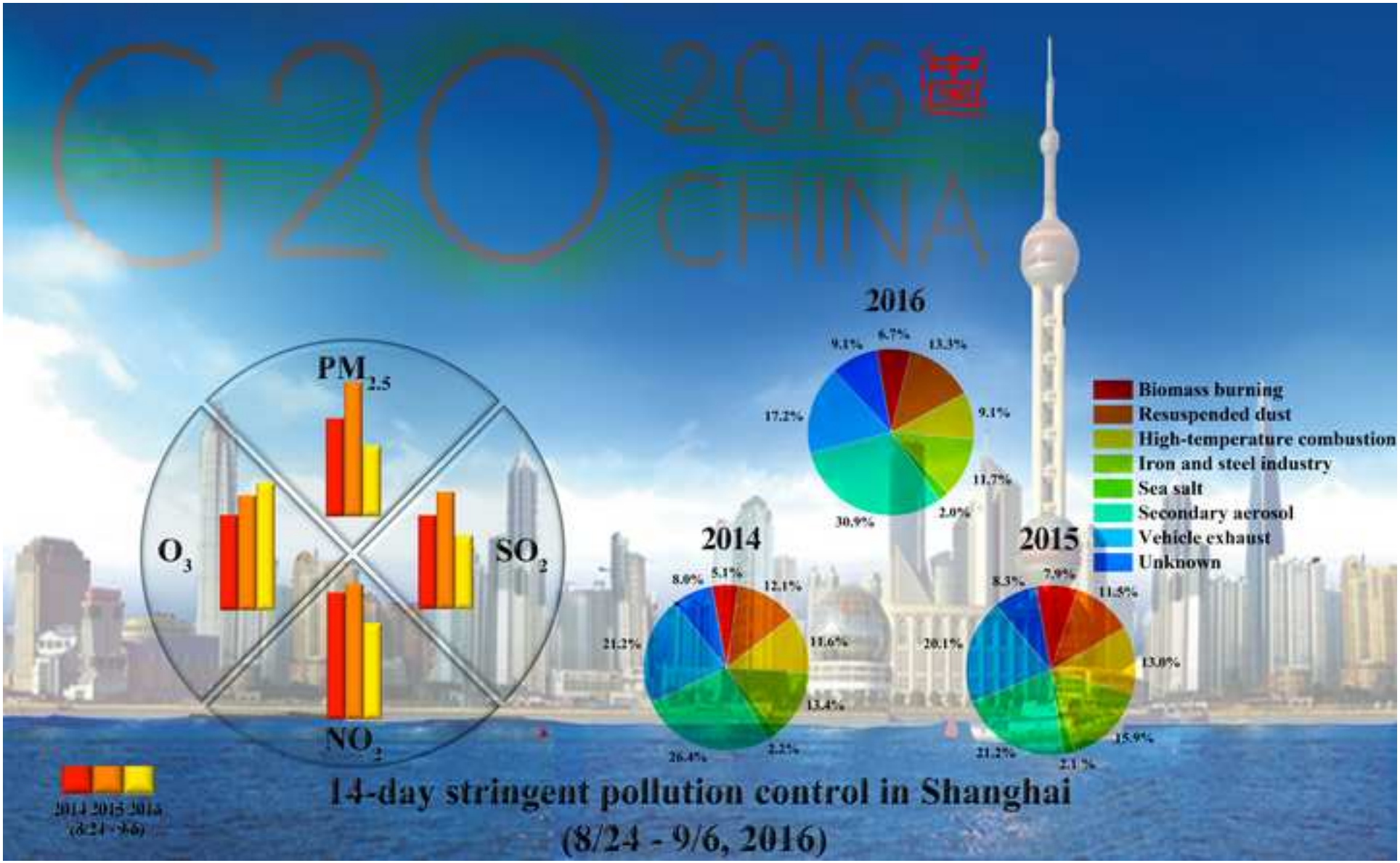

*Highlights (for review : 3 to 5 bullet points (maximum 85 characters including spaces per bullet point)

Characteristics of Atmospheric $PM_{2.5}$ Composition during the Implementation of Stringent Pollution Control Measures in Shanghai for the 2016 G20 Summit (HIGHLIGHTS)

- Effectiveness of the pollution control measures was evaluated for the G20 summit.
- Concentrations of most of criteria air pollutants reduced whereas O_3 elevated.
- Impacts of local emissions and regional transport were analyzed at two Supersites.
- Secondary aerosols and vehicle exhaust remained the top two sources of $PM_{2.5.}$

Abstract

To reduce air pollution within a 300 km radius from Hangzhou (the capital city of Zhejiang Province in East China) for the 2016 G20 summit (9/4–9/5), the 14-day (8/24–9/6) stringent pollution control measures were implemented in Shanghai. Changes in atmospheric concentrations during the same 14-day period from 2014 to 2016 were examined at two Supersites, i.e., urban Pudong site (PD) and Dianshan Lake regional site (DSL). Up to 50% reductions were found for $PM_{2.5}$, with 13.1% and 9.7% reductions for SO_2 and NO_2, respectively. No apparent improvements were found for 8-h average O_3 concentrations. Large reductions were also found for SO_4^{2-} (51.4%), NO_3^- (68.8%), and NH_4^+ (84.4%), on average. Elevated coefficient of divergence values (0.52–0.56) suggested that pollutant sources differed at the two sites. Biomass burning, resuspended dust, combustion, iron and steel industry, sea salt, secondary aerosol, and vehicle exhaust were identified at the DSL site by Positive Matrix Factorization (PMF). Secondary aerosol and vehicle exhaust accounted for 45.7% of $PM_{2.5}$ mass, followed 11.2%–13.7% each by industry, resuspended dust, and coal and oil combustion.

Keywords: $PM_{2.5}$ composition; pollution control measures; G20 summit; Shanghai

1. Introduction

As a leading voice in China's efforts to improve air quality, Shanghai government has enhanced air quality management to reduce air pollution. The "Clean Air Action of Shanghai Municipality (2013–2017)" (Shanghai Municipal Government, 2013) was initiated only one month after the implementation of state Air Pollution Prevention and Control Action Plan (The State Council of the People's Republic of China, 2013). Coal-free zones were established in the metropolitan region (i.e., Inner Ring Road) where coal and heavy oil-fired boilers were replaced with clean energy boilers by 2015. In 2014, key industries (e.g., power plant, iron and steel, cement and flat glass industries) in Yangtze River Delta (YRD) region (Shanghai Environmental Protection Burea, 2014) were subjected to either initiate control measures or retrofit existing desulfurization, denitration, and dust removal facilities. Industrial emission standards (i.e., smoke and dust $\leq$ 10 mg/m^3, $SO_2 \leq$ 35 mg/m^3, and $NO_2 \leq$ 50 mg/m^3) are expected to be attained prior to the 2020 target schedule. Implementation of vehicle (i.e., gasoline and diesel) emission standards has been established in 2014 with complete implementation in 2016. Efforts have also been made to promote low/zero-emission electric vehicles. (Bureau of Statistics of Shanghai, 2014, 2015, 2016; Clean Air Asia, 2017)

Reductions in $PM_{2.5}$ and O_3 are not apparent over the last three years. As shown in the 2014–2016 Air Quality Index (AQI) report (see also in Fig. S1) (Shanghai Environmental Monitoing Center, 2017), high frequency of pollution in the number of non-attainment days is wholly attributed to the elevated $PM_{2.5}$ and O_3 concentrations, similar to other representative mega-cities in China (Ministry of Environmental Protection of China, 2016). The days that O_3 as the major pollutant already outnumbered PM_{10}, making it second status only to $PM_{2.5}$ in Beijing–Tianjin–Hebei (Jing–Jin–Ji) region (Wang et al., 2017; Wang et al., 2015). O_3 pollution becomes the primary issue in Pearl River Delta (PRD) region (Ling et al., 2017; Wang et al., 2016).

Hangzhou, the capital city of Zhejiang Province, hosted the eleventh international forum for the 20 governments and central bank governors (the G20 summit) on 9/4–9/5 in 2016, which became China's biggest diplomatic event of the year. The neighboring Shanghai, 175 km northwest of Hangzhou, initiated a "G20 Blue" program over the 14-day period from 8/24 to 9/6 with stringent pollution control measures (Shanghai Environmental Protection Bureau, 2016). As shown in Table S1, the 14-day control measures include the company shutdown or curtail 255 oil refinery, petrochemical, steel and other industries; reduce 30% of coal-fired boilers and other combustion facilities; stop 101 large construction activities; ban single-hull ferry boats and non-road machinery operations; restrict driving of high emitter (i.e., yellow-label) vehicles to downtown; extend public transport services and encourage flexible working schedules. These immediate control actions resulted in a record of low $PM_{2.5}$ concentration (10.6 $\mu g/m^3$) in the city center.

The "G20 Blue" program provides the opportunity to investigate changes in air pollutant emissions and ambient air concentrations and compositions. Here, the continuous 14-day (8/24–9/6) sampling and analysis of ground-based meteorology, criteria air pollutant concentrations ($PM_{2.5}$, SO_2, NO, NO_2, and O_3), as well as $PM_{2.5}$ chemical speciation were conducted at two Supersites in Shanghai, i.e., urban Pudong site (PD) and Dianshan Lake regional site (DSL). The effectiveness of the implementation of the stringent pollution control measures was evaluated during the same 14-day period from 2014 to 2016. Changes in source apportionment of $PM_{2.5}$ mass were analyzed among the three years.

2. Materials and methods

2.1. Supersite characteristics

The two Supersites (i.e., PD and DSL in Fig. 1), operated by the Shanghai Environmental Monitoring Center, are situated approximately 44 km apart and designed to characterize urban exposure and pollution transport. The urban-scale PD site (31°13′N,

121°32′E) is located in downtown Shanghai (5 km east of urban center, the People's Square); whereas the DSL regional site (31°08′N, 121°05′E) is situated in 7 km east of Dianshan Lake, adjacent to Zhejiang and Jiangsu Provinces.

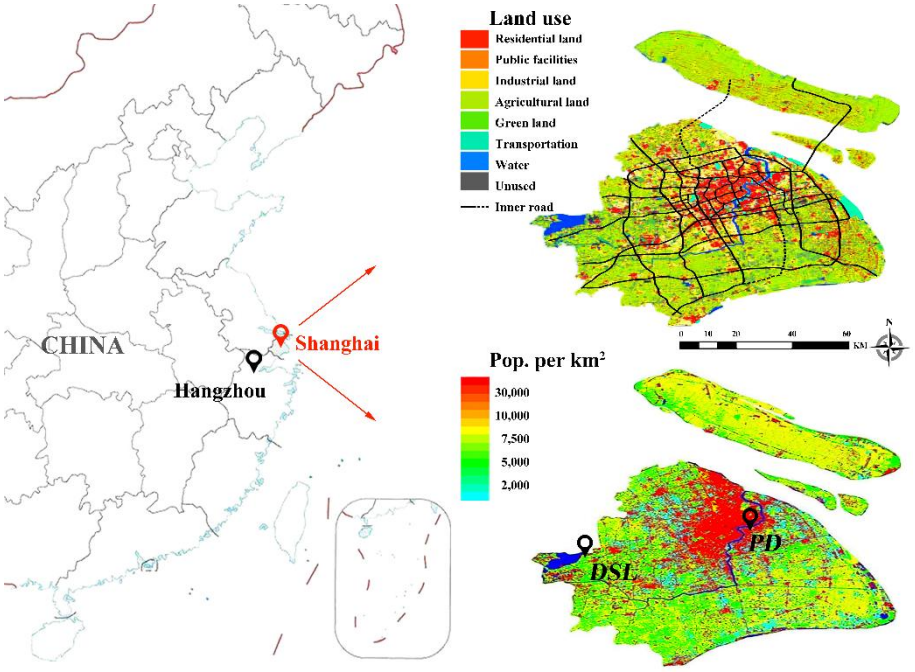

Fig. 1. Locations of the Pudong (PD) and Dianshan Lake (DSL) Supersites in Shanghai. The contour of land use and population density adopted from Shanghai statistical yearbook in 2015 (Bureau of Statistics of Shanghai, 2016).

2.2. Samples collection and analysis

$PM_{2.5}$ mass concentrations were determined by a tapered-element oscillating microbalance monitor (TEOM, Thermo FH62C–14). 24-h $PM_{2.5}$ samples were collected on quartz-fiber filters (Tissuquartz 2600 QAT, Pallflex membrane filters, USA), using a high-volume sampler (Guangzhou Mingye Huanbao Technology Company, China) with a flow rate of 1.0 m^3/h. The quartz-fiber filters were equilibrated at a constant temperature (20±1 °C) and relative humidity (40±1%) environment for 24 h before weighing. Gravitative analyses were conducted using an analytical balance (Mettler Toledo, Switzerland) with a precision of 10 μg. Detailed quality control/quality assurance (QC/QA) has been described in the literature (Chow et al., 2015; Collett, 2016; Watson et al., 2017).

Hourly $PM_{2.5}$ water-soluble inorganic species (i.e., SO_4^{2+}, NO_3^-, NH_4^+, Cl^-, K^+, Ca^{2+}, Na^+, and Mg^{2+}) and precursor gases (e.g., SO_2 and NH_3) were measured by an online MARGA (Monitor for Aerosols and Gases in Ambient Air, Model ADI2080, Metrohm Applikon BV). The MARGA system consists of a steam-jet aerosol collector with a $PM_{2.5}$ inlet where gases were removed by a wet rotating denuder and ions were captured and dissolved into the supersaturated stream before analyzed by ion chromatograph (Chow and Watson, 2017). Organic and elemental carbon (OC and EC) were acquired with an RT-4 analyzer (Sunset Lab, USA). A total of 16 trace elements (i.e., Fe, V, Cr, Mn, Co, Ni, Cu, Zn, Ga, Ge, As, Se, Cd, Au, Ba, Pb) was monitored by a continuous multi-metals monitor (Cooper Xact625) equipped with a reel-to-reel filter tape for nondestructive energy-dispersive X-ray fluorescence (EDXRF) analysis. Due to missing value (> 20 %) (Yuan et al., 2008) for trace elements at the PD site, 336 samples with 26 species at the DSL site were used for the Positive Matrix Factorization (PMF) analysis.

Nitrogen oxides were measured using a chemiluminescence $NO–NO_2–NO_x$ analyzer (EC 9841B) with a minimum detection limit of 0.4×10^{-9} (volume fraction), while O_3 were monitored using a UV spectrophotometry ozone analyzer (EC 9810B) with a minimum detection limit of 0.4×10^{-9}. Meteorological parameters including wind speed and direction, temperature, relative humidity, pressure, and rainfall were monitored by an automatic meteorological station (Met Station One Instrument, USA), which are placed 18 m above the ground level on the rooftop of each Supersite. These measurements follows the QC/QA procedure specified in the Technical Guideline of Automatic Stations of Ambient Air Quality in Shanghai, which is based on the national specification HJ/T193–2005 (Ministry of Environmental Protection of China, 2005) and HJ/193–2013 (Ministry of Environmental Protection of China, 2013).

3. Results and discussion

3.1 Meteorological conditions and atmospheric pollutant concentrations

Fig. 2a–b show that the daily meteorological phenomena were similar among the three years with a few exception. Temperatures remained moderate (26.8 °C) with low average relative humidity (74%) except for the period of 8/28–8/30 in 2016. Atmospheric pressures were lower during 8/29–9/1 in 2016. Wind speed was remaining low, averaging 1.9 m/s, consistent with the 168-h back trajectories (see also in Fig. S2). The predominant northwesterly winds from 2014 to 2016 were 50.3%, 47.4%, and 44.1% at the PD site, and 48.8%, 41.6%, and 43.5% at the DSL site, respectively. Therefore, meteorological conditions during the 2016 G20 period were not atypical, indicating that comparisons of air pollutant concentrations can be made among the three years.

In the autumn harvest period, biomass burning can emit more than 60% of trace gases and particles emissions in the YRD region (Zha et al., 2013). Hence, Shanghai usually suffers from the greater impact of the pollutant transport from its adjacent Provinces. More abundant active fires still existed in 2016 from the neighboring regions which somewhat affect the pollution condition in Shanghai (see also in Fig. S3).

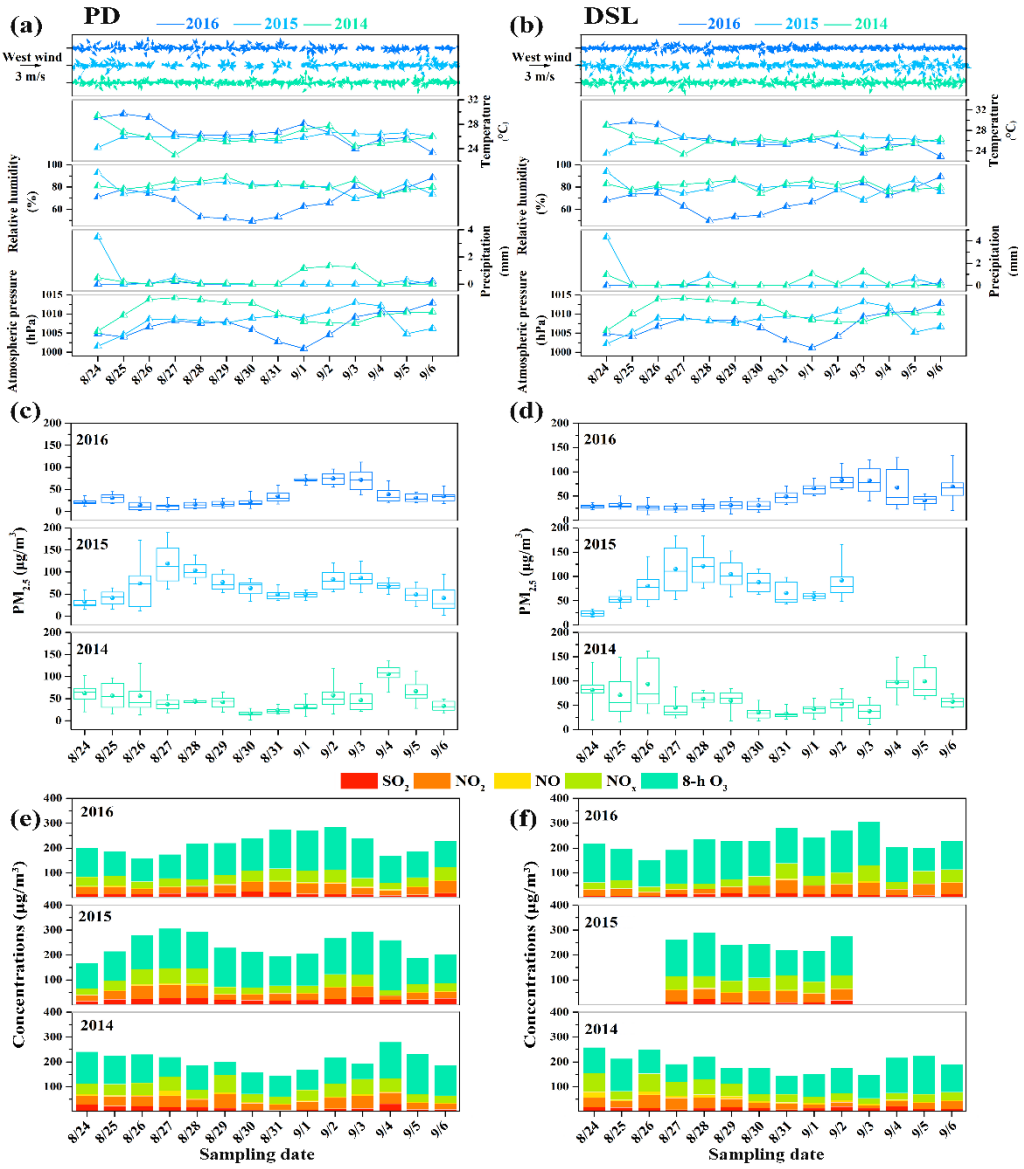

Fig. 2. Comparison of meteorological parameters, $PM_{2.5}$ concentrations (Box-and-Whisker Plot), and trace gaseous pollutants at the PD (a, c, and e) and DSL (b, d, and f) sites during the same period (8/24–9/6) from 2014 to 2016. A Box-and-Whisker plot: the mean (a black sphere), the median (a horizontal line in the box), the 25th percentile (the bottom edge of the box), the 75th percentile (represented by the top edge of the box), the minimum (the bottom edge of the whisker) and the maximum (the top edge of the whisker).

Fig. 2c–d show higher reductions in $PM_{2.5}$ during the 2016 G20 period. Daily $PM_{2.5}$ concentrations during 8/24–8/31 were low, averaging 24.0 μg/m^3 with a minimum of 10.6 μg/m^3 at PD, about 61.0% and 40.8% lower than these found in 2015 and 2014, respectively.

Lower $PM_{2.5}$ concentrations were also found for the DSL site during the last week of August in 2016, averaging 31.2 μg/m^3 with a minimum of 16.0 μg/m^3, about 66.0% and 48.6% lower than 2015 and 2014, respectively. The prevailing northwestly winds enhanced the diffusion of air pollutants. Prior to the commencement of G20 (9/2–9/3), $PM_{2.5}$ concentrations increased to 74.8 μg/m^3 at PD and 81.6 μg/m^3 at DSL with some decreases on 9/4–9/6 in 2016. The DSL reginal site, is surrounded with green and agricultural lands in Fig.1, suffered pollutant transport from the neighboring regions with clockwise transport from northwesterly to northeasterly (see also in Fig. S2), contributing to a rise of pollutant concentrations.

Gaseous comparison excluded CO as CO concentrations remain below the Chinese National Ambient Air Quality Standards (NAAQS) in recent years (Clean Air Asia, 2017). Not much changes in annual SO_2 concentrations ranged from 18.9 μg/m^3 in 2014 to 15.9 μg/m^3 in 2016, below the NAAQS First Standard of 20 μg/m^3. Annual NO_2 concentrations ranged from 42.1 μg/m^3 in 2014 to 40.6 μg/m^3 in 2016, close to the NAAQS of 40 μg/m^3. Consequently, no apparent changes in SO_2 were found during the same 14-day from 2014 to 2016 in Fig. 2e–f, with an average of 15.1 μg/m^3 in 2014, 21.8 μg/m^3 in 2015, and 16.6 μg/m^3 in 2016 at the PD site and 14.3 μg/m^3 in 2014, 13.0 μg/m^3 in 2015, and 12.8 μg/m^3 in 2016 at the DSL site. Due to regional transport by the prevailing northwesterly winds, concentrations of SO_2 at PD were slightly higher than DSL, while NO_2 at PD was 9.4% higher than that at DSL, reflecting the impact of motor vehicle emissions in urban areas.

On the contrary, concentrations of 8-h O_3 elevated to higher instead of dropping during the G20 period, with higher increases found at the PD site as compared to DSL. This is consistent with those reported in recent studies (Li et al., 2018; Wang et al., 2015; Zhao et al., 2018), where inhibition of NO_x on O_3 was more significant in urban areas.

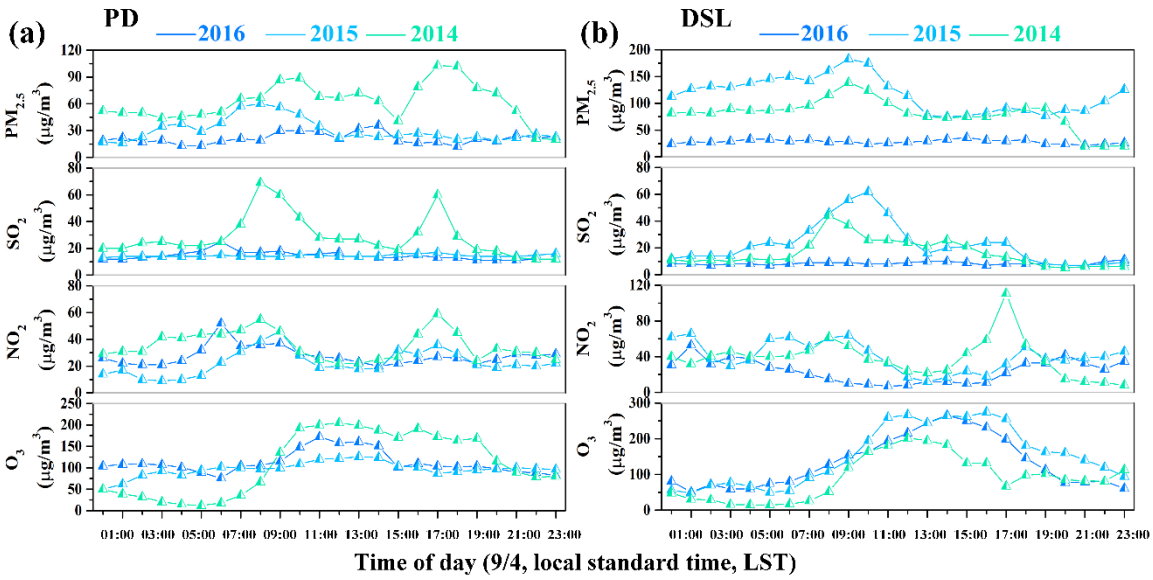

Fig. 3. Diurnal variations of $PM_{2.5}$, SO_2, NO_2, and O_3 at the PD (a) and DSL (b) sites on 9/4 from 2014 to 2016.

The diurnal variations on 9/4 (the first day of the 2016 G20 summit) of air pollutants were compared in Fig. 3. It is obvious that rush-hour peaks for $PM_{2.5}$, SO_2, and NO_2 found in 2014 and 2015 were diminished in 2016. $PM_{2.5}$ and SO_2 concentrations remained low throughout the day at the PD and DSL sites. Different diurnal patterns were found for NO_2, peaked at 07:00 and 18:00 LST during the rush-hour traffic at the PD site but remained relatively lower (< 40 μg/m^3) at the DSL site with accommodation found during late evening (23:00 LST) to early morning (02:00 LST). Concentrations of ground level O_3 were affected by temperature, namely, high temperature in the daytime was favorable for O_3 formation (Xue et al., 2014). Diurnal curves of all monitored pollutants except for O_3 in the G20 period were lower than those found in the previous two years.

3.2 Changes in chemical composition of $PM_{2.5}$

3.2.1 Water–soluble inorganic ions and carbonaceous species

In Fig. 4a–b, concentrations of chemical composition of $PM_{2.5}$ decreased during the 14-day period in 2016 and their reductions varied between the PD and DSL sites. Total water-

198 soluble inorganic ions (TWSIIs) concentrations averaged 9.69 μg/m^3 at PD and 13.0 μg/m^3 at
199 DSL, which accounted for 56.2% and 52.3% of $PM_{2.5}$ mass in the G20 period (see also in Fig.
200 S4). Compared with the previous two years, TWSIIs decreased by at an average of 57.5% and
201 44.0% at PD and DSL, respectively. As for main secondary ionic aerosols (SIA), sulfate
202 SO_4^{2-}, nitrate NO_3^-, and ammonium NH_4^+ (SNA), averagely 41.5%, 68.8%, and 76.5% of
203 reductions were attained at PD and just 28.9% 29.5%, and 26.0% at DSL. SNA shared 88.3%
204 of TWSIIs at PD and 86.8% at DSL among the three years. Strong correlations between SIA
205 and $PM_{2.5}$ were observed at the PD ($R = 0.87$, $n = 336$, $p < 0.01$) and DSL ($R = 0.82$, $n = 336$,
206 $p < 0.01$) sites, respectively. These findings denoted that NO_3^-, SO_4^{2-} and NH_4^+ were the
207 major ions in $PM_{2.5}$ and SIA variations were associated with the formation, transportation and
208 removal of $PM_{2.5}$.

209 No massive reduction in K^+ concentrations was at the PD site from 0.25 μg/m^3 to 0.19
210 μg/m^3; whereas banning burning activities contributed to up to 89.6% reductions at the DSL
211 site. Fig. 4b shows apparent reduction of 44.2% for NH_4^+ at the DSL site, suggesting the
212 effectiveness of precursor NH_3 emissions control from agricultural activities (Xu et al., 2015;
213 Zhang et al., 2018). However, NH_4^+ exists in compound form through the combination of
214 SO_4^{2-} and NO_3^-. It is possible that the reductions of SO_4^{2-} and NO_3^- are associated with the
215 NH_4^+ decreases (Collett, 2016; Zhang et al., 2018) in the urban environment and the higher
216 concentrations of NH_4^+ at the regional DSL are complicated rather than singly from the local.

217 Na^+ concentrations at the PD site were 5 times higher than those at DSL, implying the
218 impact from sea salt at the urban site in Shanghai (Qiao et al., 2016). Reductions of Na^+, Ca^{2+},
219 and Mg^{2+} corresponded to dust controls in construction activities and steel sweeping (Xiu et
220 al., 2004; Zhang et al., 2015). Water soluble Ca^{2+} accounted for 1.7% to 2.0% of TWSIIs,
221 lower than the 6.8% in Wuhan (Zhang et al., 2015), 4.0% in Zhengzhou (Geng et al., 2013),
222 and 2.6% in Xiamen (Zhang et al., 2012). Weak correlations were found for Ca^{2+} between the

PD and DSL sites ($R = 0.28$, $n = 336$, $p < 0.05$), suggesting differences in geological composition between the urban and regional areas. Yang et al. (2018) reports high Cl^-/Na^+ ratios (2.46–5.0) in northern and western China. These ratios were about an order of magnitude higher than those found at PD (0.44) but similar to 2.31 found at DSL. The lower Cl^-/Na^+ ratio at PD could be ascribed by curtailing coal-oriented consumptions in urban Shanghai (He et al., 2001).

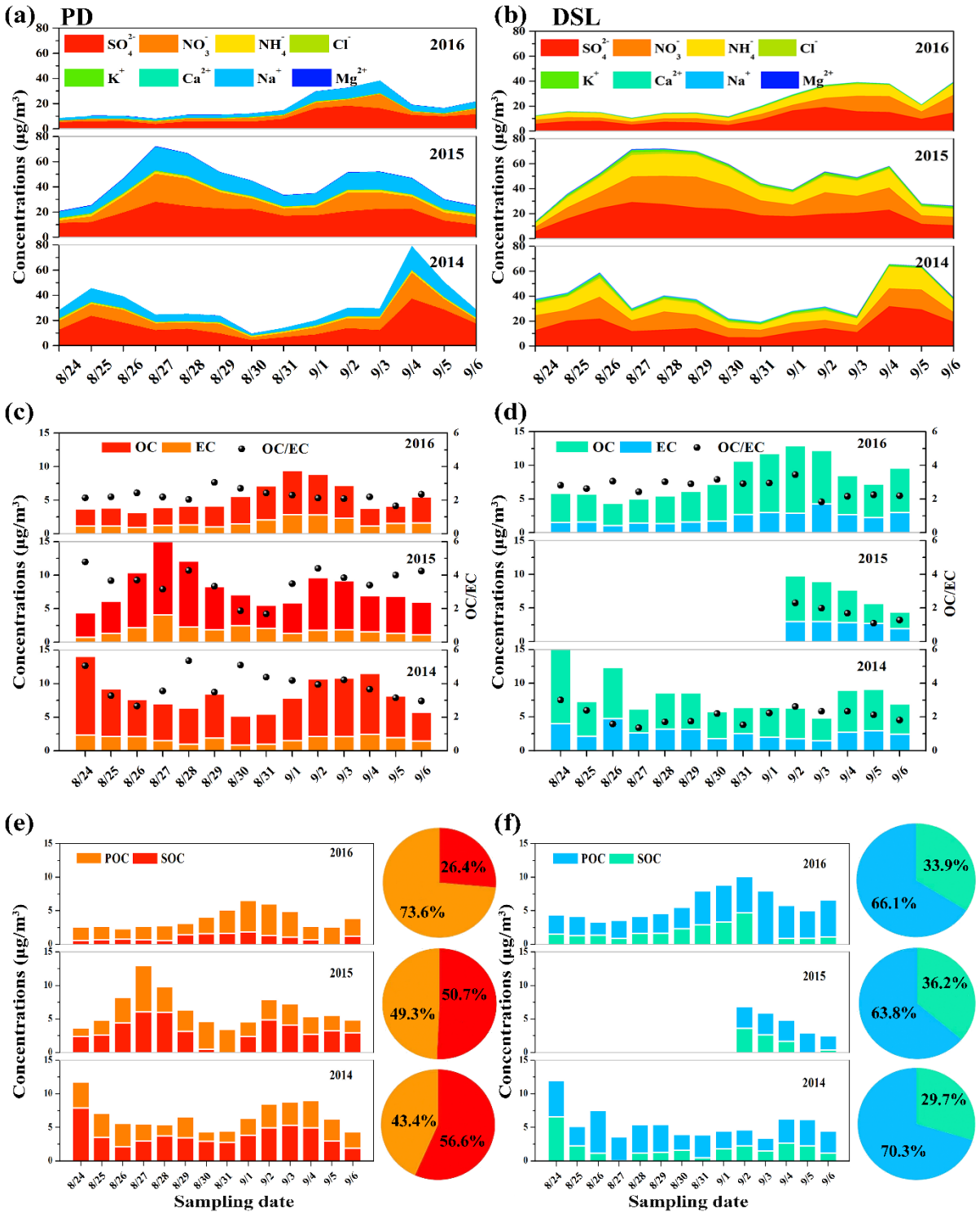

Fig. 4. Comparison of water-soluble inorganic ions (WSIIs) (a and b), carbonaceous species (c and d), and SOC estimation (e and f) in $PM_{2.5}$ at the PD and DSL sites during the same period (8/24–9/6) from 2014 to 2016. Pie charts (inset of e and f): changes in the fractions of POC and SOC in OC concentrations at both sites.

Carbonaceous aerosol (TC) is the major component of $PM_{2.5}$ and consists of two components, i.e., organic carbon (OC) and elemental carbon (EC). OC could be divided into primary organic carbon (POC) and secondary organic carbon (SOC). POC is emitted directly in the particle-phase and SOC is formed from gas-to-particle conversion in the atmosphere. The presence of SOC can be estimated by the minimum OC/EC ratio (Huang et al., 2012; Zhang et al., 2012):

$$POC = EC \times \left(\frac{OC}{EC}\right)_{min} \quad (1)$$

$$SOC = OC - POC \quad (2)$$

Where $(OC/EC)_{min}$ is the minimum OC/EC ratio. The concentrations of OC (POC and SOC) and EC, as well as OC/EC ratios of $PM_{2.5}$ at the PD and DSL sites are illustrated in Fig. 4c–f. Average TC concentrations were 3.51 μg/m^3 and 6.03 μg/m^3 during the 14-day period in 2016 and accounted for 14.5% and 19.3% of $PM_{2.5}$ mass (see also in Fig. S4) at PD and DSL, respectively. OC accounted for 71.0%–77.2% of TC, ranging from 7.13 μg/m^3 to 7.39 μg/m^3 at PD and 1.85 μg/m^3 to 2.19 μg/m^3 at DSL during the same 14-day period from 2014 to 2016.

Good correlations were found between OC and K^+ ($R = 0.97$, $n = 336$, $p < 0.01$) at the DSL site, suggesting their common emission sources (Li et al., 2015) and the association with fire events (see also in Fig. S3). In Fig. 4c–d, average OC/EC ratios decreased from 3.9 in 2014, 3.6 in 2015 to 2.2 in 2016 at the PD site, more pronounced than those found at the DSL site from 2.7 in 2014 to 2.1 in 2016. In Fig. 4e−f, average SOC during the G20 period were 2.7 μg/m^3 and 3.6 μg/m^3, accounted for 26.4% and 33.9% of OC at the PD and DSL sites, respectively. The SOC/OC ratios shared less variations at DSL (29.7% to 36.2%) than PD (26.4% to 56.6%). $PM_{2.5}$ shows higher correlations with SOC ($R = 0.85$, $n = 336$, $p < 0.01$) at PD and ($R = 0.75$, $n = 336$, $p < 0.01$) at DSL than with POC ($R = 0.53$, $n = 60$, $p < 0.01$) at PD and ($R = 0.66$, $n = 336$, $p < 0.01$) at DSL. These findings reflect that organic components in the atmosphere were related to the formation, transportation and removal of $PM_{2.5}$ in

Shanghai (Huang et al., 2012; Liang et al., 2016). Large reductions in SOC/OC ratios at the PD site during the G20 period were more pronounced than those found at DSL. Weak correlations between OC and EC ($R = 0.32$, $n = 336$, $p < 0.05$) at PD and ($R = 0.28$, $n = 336$, $p < 0.05$) at DSL indicate that they derived from different sources (Li et al., 2012; Tao et al., 2014).

3.2.2 Divergence analysis between two sites

Coefficient of divergence (CD) can be utilized to characterize the differences of chemical components between the two sampling sites, calculated by the following equation (Zhang and Friedlander, 2000):

$$CD_{AB} = \sqrt{\frac{1}{n}\sum_{i=1}^{n}\left(\frac{C_{iA} - C_{iB}}{C_{iA} + C_{iB}}\right)^2} \quad (3)$$

Where C_{iA} and C_{iB} represent the concentrations of component i at site A and site B, respectively. If the CD is approximate to 0.00, the emission sources between the two sites are similar; whereas close to 1.00, the two sites are different (Zhang and Friedlander, 2000). This approach was adopted by (Yang et al., 2002) in Beijing (CD = 0.064) and (Zhang et al., 2015) in Wuhan (CD = 0.098), indicating that the similarity of $PM_{2.5}$ compositions. In contrast, the values of CDs between PD and DSL ranged 0.52−0.56 from 2014 to 2016 as shown in Fig. 5., which supports the investigation of the complicated impacts between urban and regional sites.

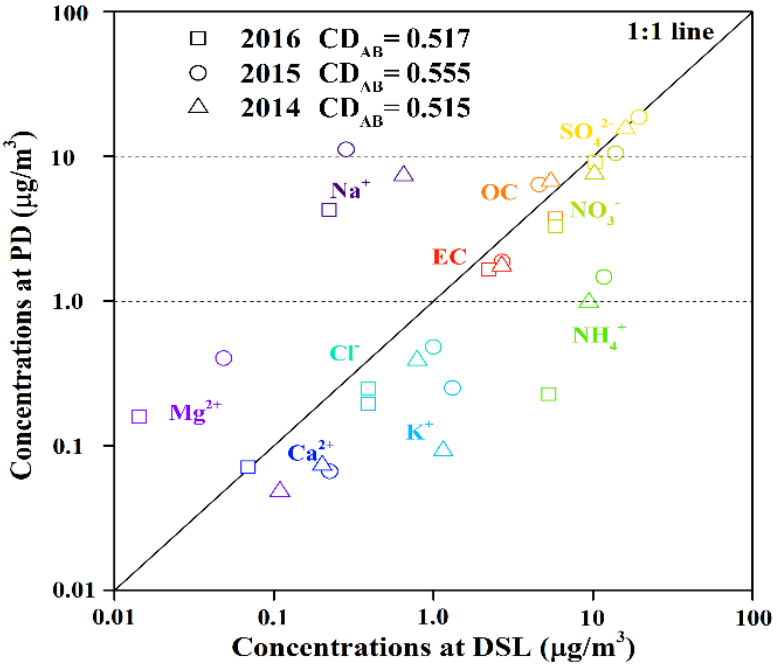

273

274 **Fig. 5.** Coefficient of divergence (CD) that characterizes the differences of $PM_{2.5}$ chemical
275 components between PD and DSL during the same period (8/24–9/6) from 2014 to 2016.

276 **4. Effectiveness of the pollution control measures**

277 Annual mean concentrations of $PM_{2.5}$, SO_2, and NO_2 reduced by 14.1%, 21.9%, and
278 11.4%, respectively, in 2016 as compared to 2014 and 2015. Though the 14-day pollution
279 control measures imposed during the G20 period, concentrations of $PM_{2.5}$ mass, carbon, and
280 ions (especially SO_4^{2+}, NO_3^-, and NH_4^+) decreased significantly as compared to the same
281 period in the previous two years shown in Fig.6. Higher number of the air quality attainment
282 days were achieved (see also in Fig. S5). No improvement was found for O_3 at either the PD
283 or DSL sites.

284

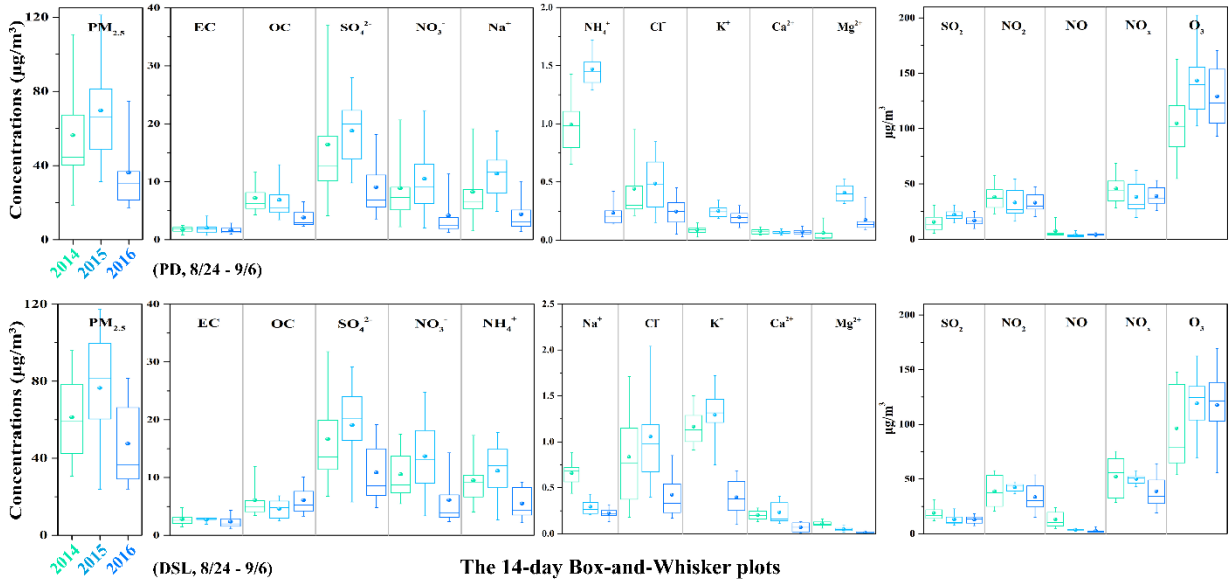

285

286 **Fig. 6.** Comparison of concentrations of air pollutants ($PM_{2.5}$ mass, carbon, ions and trace
287 gaseous pollutants) at the PD (a) and DSL (b) sites during the same period (8/24–9/6) from
288 2014 to 2016.

289 Seven sources were identified by the Positive Matrix Factorization (PMF) model (see
290 also in Fig. S6) for $PM_{2.5}$ samples at the DSL site, including biomass burning, resuspended
291 dust, high-temperature combustion, iron and steel industry, sea salt, secondary aerosol, and
292 vehicle exhaust. Figs. 7 shows changes in temporal variations in $PM_{2.5}$ and source
293 contribution among the three years. The two largest contributors were secondary aerosols and
294 vehicle exhaust among the three years, which accounted for 45.7% of $PM_{2.5}$ mass, followed
295 by iron and steel industry (13.7%), resuspended dust (12.3%), and high-temperature
296 combustion from coal and oil boilers (11.2%). Biomass burning ranged from 5.1% to 7.9% of
297 $PM_{2.5}$ and was attributed to the prevailing northwesterly transports, also suppoted by the back
298 trajactories (see also in Fig. S2) and active fire detections (see also in Fig. S3).

299

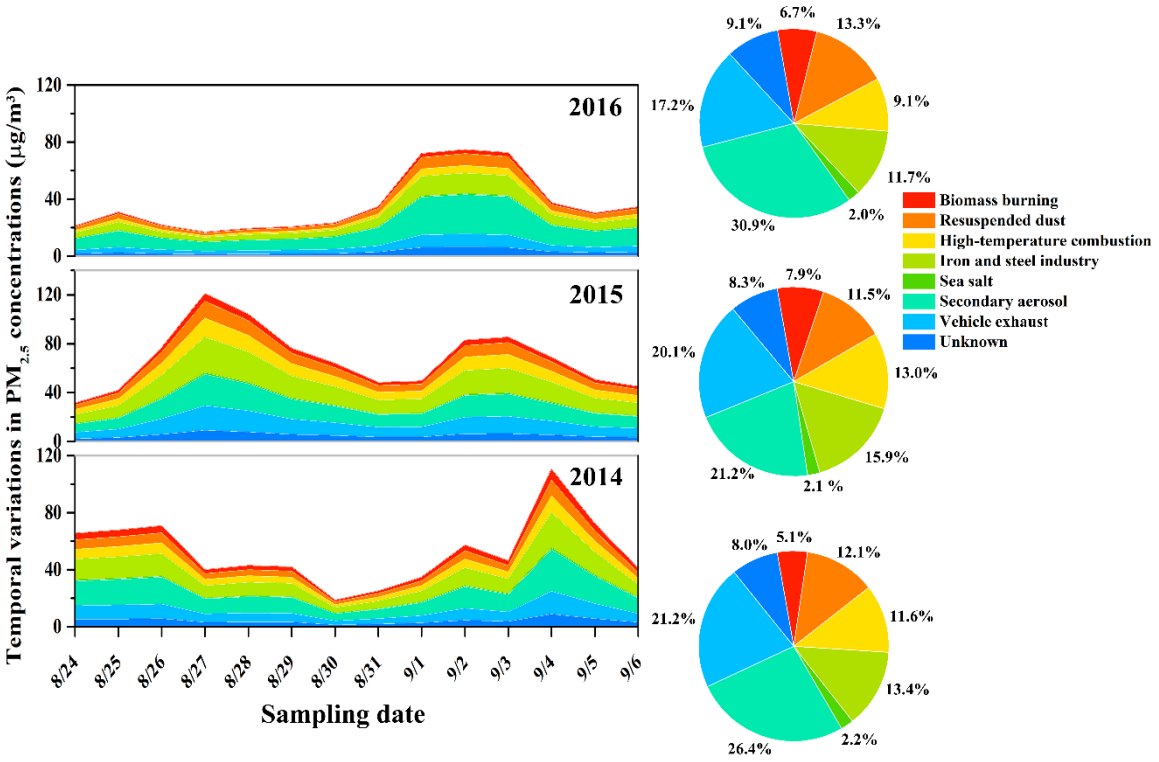

Fig. 7. Changes in source apportionment resolved from $PM_{2.5}$ samples at the DSL site during the same period (8/24–9/6) from 2014 to 2016.

5. Conclusions

Implementation of stringent pollution control measures over the 14-day period resulted in large reduction in pollution concentrations. The effectiveness of the pollution control in the urban center was more pronounced than regional areas. If the onset of unfavorable meteorological conditions is forecasted, the enhanced reduction measures would be implemented several days ahead of pollution episodes. Since the impact of multiple pollutants on $PM_{2.5}$ and O_3 concentrations and atmospheric oxidation capacity is nonlinear and complicated, reduction in precursor gases (e.g., SO_2, NO_x, NH_3 and VOCs) should be synergistically strengthened for the next stage. However, its long-term impacts on ambient concentration levels need to be further evaluated. A market-based approach needs to be examined to evaluate the cost of an ad-hoc closures of industries. The profit and loss between the environment and business need to be balanced.

Acknowledgements

This research was financially supported by The Ministry of Science and Technology of China (2013FY112700 and 2014BAC22B07), Science and Technology Commission of Shanghai (Project No. 14DZ1202900), The Research Grants Council of Hong Kong Government (Project No. T24/504/17), The Research Grants Council of Hong Kong Government (PolyU152083/14E and PolyU152090/15E), and Hong Kong RGC Collaborative Research Fund (C5022–14G).

Appendix A. Supplementary Information

Supplementary Information associated with this article can be found in this section, including: 14-day pollution control measures, distribution of Air Quality Index (AQI) in Shanghai from 2014 to 2016, NOAA HYSPLIT trajectory model results, active fire detection in neighboring regions, fractional abundance of five major species of $PM_{2.5}$, changes in air quality attainment during the G20 period, and source identification $PM_{2.5}$ samples using PMF model.

Notes

The authors declare no competing financial interest.

References

Bureau of Statistics of Shanghai (BBS), 2014. Shanghai Statistical Yearbook 2013. China Statistics Press, Beijing (in Chinese).

Bureau of Statistics of Shanghai (BBS), 2015. Shanghai Statistical Yearbook 2014. China Statistics Press, Beijing (in Chinese).

Bureau of Statistics of Shanghai (BBS), 2016. Shanghai Statistical Yearbook 2015. China Statistics Press, Beijing (in Chinese).

Chow, J.C., Wang, X., Sumlin, B.J., Gronstal, S.B., Chen, L.-W.A., Trimble, D.L., Kohl, S.D., Mayorga, S.R., Riggio, G., and Hurbain, P.R., 2015. Optical calibration and equivalence of a multiwavelength thermal/optical carbon analyzer. Aerosol Air Qual. Res. *15*, 1145.

Chow, J.C., and Watson, J.G., 2017. Enhanced ion chromatographic speciation of water-soluble $PM_{2.5}$ to improve aerosol source apportionment. Aerosol Sci. Eng. *1*, 7-24.

Clean Air Asia (CAA), 2017. China Air 2016–air pollution prevention and control progress in Chinese cities.

Collett, J.L., 2016. The importance of vehicle emissions as a source of atmospheric ammonia in the megacity of Shanghai. Atmos. Chem. Phys. *16*, 3577.

Geng, N., Wang, J., Xu, Y., Zhang, W., Chen, C., and Zhang, R., 2013. $PM_{2.5}$ in an industrial district of Zhengzhou, China: chemical composition and source apportionment. Particuology *11*, 99–109.

He, K., Yang, F., Ma, Y., Zhang, Q., Yao, X., Chan, C.K., Cadle, S., Chan, T., and Mulawa, P., 2001. The characteristics of $PM_{2.5}$ in Beijing, China. Atmos. Environ. *35*, 4959–4970.

354 Huang, H., Ho, K., Lee, S., Tsang, P., Ho, S.S.H., Zou, C., Zou, S., Cao, J., and Xu, H., 2012.
355 Characteristics of carbonaceous aerosol in $PM_{2.5}$: Pearl Delta River region, China.
356 Atmos. Res. *104*, 227–236.
357 Li, B., Zhang, J., Zhao, Y., Yuan, S., Zhao, Q., Shen, G., and Wu, H., 2015. Seasonal
358 variation of urban carbonaceous aerosols in a typical city Nanjing in Yangtze River
359 Delta, China. Atmos. Environ. *106*, 223-231.
360 Li, Y.-C., Yu, J.Z., Ho, S.S.H., Yuan, Z., Lau, A.K., and Huang, X.-F., 2012. Chemical
361 characteristics of $PM_{2.5}$ and organic aerosol source analysis during cold front episodes in
362 Hong Kong, China. Atmos. Res. *118*, 41–51.
363 Li, Z., Xue, L., Yang, X., Zha, Q., Tham, Y.J., Yan, C., Louie, P.K., Luk, C.W., Wang, T.,
364 and Wang, W., 2018. Oxidizing capacity of the rural atmosphere in Hong Kong,
365 Southern China. Sci. Total Environ. *612*, 1114–1122.
366 Liang, C.-S., Duan, F.-K., He, K.-B., and Ma, Y.-L., 2016. Review on recent progress in
367 observations, source identifications and countermeasures of $PM_{2.5}$. Environ. Int. *86*,
368 150–170.
369 Ling, Z., Zhao, J., Fan, S., and Wang, X., 2017. Sources of formaldehyde and their
370 contributions to photochemical O_3 formation at an urban site in the Pearl River Delta,
371 southern China. Chemosphere *168*, 1293–1301.
372 Ministry of Environmental Protection of China (MEP), 2005. Automated Methods for
373 Ambient Air Quality Monitoring (HJ/T193–2005).
374 Ministry of Environmental Protection of China (MEP), 2013. Technical Specifications for
375 Installation and Acceptance of Ambient Air Quality Continuous Automated Monitoring
376 System for SO_2, NO_2, O_3 and CO (HJ193–2013).
377 Ministry of Environmental Protection of China (MEP), 2016. Urban Ambient Air Quality
378 Daily Report. http://www.mep.gov.cn/hjzl/ (in Chinese).

Qiao, T., Zhao, M., Xiu, G., and Yu, J., 2016. Simultaneous monitoring and compositions analysis of PM_1 and $PM_{2.5}$ in Shanghai: implications for characterization of haze pollution and source apportionment. Sci. Total Environ. *557*, 386-394.

Shanghai Environmental Protection Bureau (SEPB), 2014. Air Pollution Prevention and Control Plan for Key Industries in Yangtze River Delta.

Shanghai Environmental Monitoing Center (SEMC), 2017. Real-time Air Quality Reporting System in Shanghai.

Shanghai Environmental Protection Bureau (SEPB), 2016. The G20 air pollution control program in Shanghai (in Chinese).

Shanghai Municipal Government (SMG), 2013. Clean Air Action of Shanghai Municipality (2013–2017) (in Chinese).

Tao, J., Gao, J., Zhang, L., Zhang, R., Che, H., Zhang, Z., Lin, Z., Jing, J., Cao, J., and Hsu, S.-C., 2014. $PM_{2.5}$ pollution in a megacity of southwest China: source apportionment and implication. Atmos. Chem. Phys. *14*, 8679–8699.

The State Council of the People's Republic of China, 2013. Air Pollution Prevention and Control Action Plan (in Chinese).

Wang, N., Lyu, X., Deng, X., Guo, H., Deng, T., Li, Y., Yin, C., Li, F., and Wang, S., 2016. Assessment of regional air quality resulting from emission control in the Pearl River Delta region, southern China. Sci. Total Environ. *573*, 1554–1565.

Wang, T., Xue, L., Brimblecombe, P., Lam, Y.F., Li, L., and Zhang, L., 2017. Ozone pollution in China: a review of concentrations, meteorological influences, chemical precursors, and effects. Sci. Total Environ. *575*, 1582–1596.

Wang, Z., Li, Y., Chen, T., Li, L., Liu, B., Zhang, D., Sun, F., Wei, Q., Jiang, L., and Pan, L., 2015b. Changes in atmospheric composition during the 2014 APEC conference in Beijing. J. Geophys. Res.: Atmos. *120*, 12695-12707.

Watson, J.G., Tropp, R.J., Kohl, S.D., Wang, X., and Chow, J.C., 2017. Filter processing and gravimetric analysis for suspended particulate matter samples. Aerosol Sci. Eng. *1*, 93-105.

Xiu, G., Zhang, D., Chen, J., Huang, X., Chen, Z., Guo, H., and Pan, J., 2004. Characterization of major water-soluble inorganic ions in size-fractionated particulate matters in Shanghai campus ambient air. Atmos. Environ. *38*, 227–236.

Xu, P., Zhang, Y., Gong, W., Hou, X., Kroeze, C., Gao, W., Luan, S., 2015. An inventory of the emission of ammonia from agricultural fertilizer application in China for 2010 and its high-resolution spatial distribution. Atmos. Environ. *115*, 141-148.

Xue, L., Wang, T., Louie, P.K., Luk, C.W., Blake, D.R., and Xu, Z., 2014. Increasing external effects negate local efforts to control ozone air pollution: a case study of Hong Kong and implications for other Chinese cities. Environ. Sci. Technol. *48*, 10769–10775.

Yang, F., He, K., Ma, Y., Zhang, Q., Yao, X., Chan, C.K., Cadle, S., Chan, T., and Mulawa, P., 2002. Chemical characteristics of $PM_{2.5}$ species in Beijing ambient air. J. Tsinghua Univ. (Sci. Technol.) *42*, 1605–1608.

Yang, X., Wang, T., Xia, M., Gao, X., Li, Q., Zhang, N., Gao, Y., Lee, S., Wang, X., and Xue, L., 2018. Abundance and origin of fine particulate chloride in continental China. Sci. Total Environ. *624*, 1041–1051.

Yuan, H., Zhuang, G., Li, J., Wang, Z., Li, J., 2008. Mixing of mineral with pollution aerosols in dust season in Beijing: Revealed by source apportionment study. Atmos. Environ. *42*, 2141-2157.

Zha, S., Zhang, S., Cheng, T., Chen, J., Huang, G., Li, X., and Wang, Q., 2013. Agricultural fires and their potential impacts on regional air quality over China. Aerosol Air Qual. Res. *13*, 992–1001.

Zhang, F., Wang, Z.-w., Cheng, H.-r., Lv, X.-p., Gong, W., Wang, X.-m., and Zhang, G. (2015). Seasonal variations and chemical characteristics of $PM_{2.5}$ in Wuhan, central China. Sci. Total Environ. *518*, 97–105.

Zhang, F., Xu, L., Chen, J., Yu, Y., Niu, Z., and Yin, L., 2012. Chemical compositions and extinction coefficients of $PM_{2.5}$ in peri-urban of Xiamen, China, during June 2009–May 2010. Atmos. Res. *106*, 150–158.

Zhang, L., Chen, Y., Zhao, Y., Henze, D.K., Zhu, L., Song, Y., Paulot, F., Liu, X., Pan, Y., and Lin, Y., 2018. Agricultural ammonia emissions in China: reconciling bottom-up and top-down estimates. Atmos. Chem. Phys. *18*, 339.

Zhang, Z., and Friedlander, S.K., 2000. A comparative study of chemical databases for fine particle Chinese aerosols. Environ. Sci. Technol. *34*, 4687–4694.

Zhao, S., Yu, Y., Yin, D., Qin, D., He, J., and Dong, L., 2018. Spatial patterns and temporal variations of six criteria air pollutants during 2015 to 2017 in the city clusters of Sichuan Basin, China. Sci. Total Environ. *624*, 540–557.

Figure Captions

Fig. 1. Locations of the Pudong (PD) and Dianshan Lake (DSL) Supersites in Shanghai. The contour of land use and population density adopted from Shanghai statistical yearbook in 2015 (Bureau of Statistics of Shanghai, 2016).

Fig. 2. Comparison of meteorological parameters, $PM_{2.5}$ concentrations (Box-and-Whisker Plot), and trace gaseous pollutants at the PD (a, c, and e) and DSL (b, d, and f) sites during the same period (8/24–9/6) from 2014 to 2016. A Box-and-Whisker plot: the mean (a black sphere), the median (a horizontal line in the box), the 25^{th} percentile (the bottom edge of the box), the 75^{th} percentile (represented by the top edge of the box), the minimum (the bottom edge of the whisker) and the maximum (the top edge of the whisker).

Fig. 3. Diurnal variations of $PM_{2.5}$, SO_2, NO_2, and O_3 at the PD (a) and DSL (b) sites on 9/4 from 2014 to 2016.

Fig. 4. Comparison of water-soluble inorganic ions (WSIIs) (a and b), carbonaceous species (c and d), and SOC estimation (e and f) in $PM_{2.5}$ at the PD and DSL sites during the same period (8/24–9/6) from 2014 to 2016. Pie charts (inset of e and f): changes in the fractions of POC and SOC in OC concentrations at both sites.

Fig. 5. Coefficient of divergence (CD) that characterizes the differences of $PM_{2.5}$ chemical components between PD and DSL during the same period (8/24–9/6) from 2014 to 2016.

Fig. 6. Comparison of concentrations of air pollutants ($PM_{2.5}$ mass, carbon, ions and trace gaseous pollutants) at the PD (a) and DSL (b) sites during the same period (8/24–9/6) from 2014 to 2016.

Fig. 7. Changes in source apportionment resolved from $PM_{2.5}$ samples at the DSL site during the same period (8/24–9/6) from 2014 to 2016.

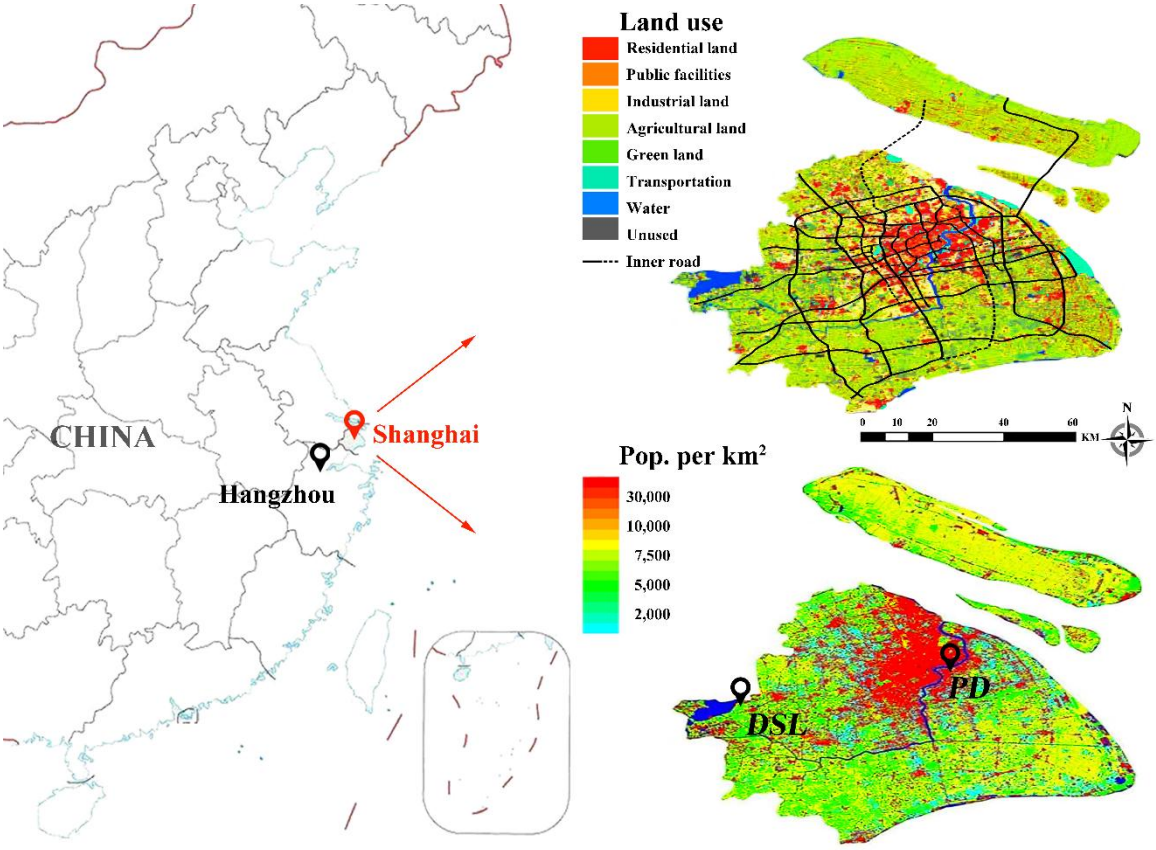
CHINA
Shanghai
Hangzhou
Land use
Residential land
Public facilities
Industrial land
Agricultural land
Green land
Transportation
Water
Unused
Inner road
0 10 20 40 60
KM
N
Pop. per km²
30,000
10,000
7,500
5,000
2,000
PD
DSL

467

468 **Fig.1**

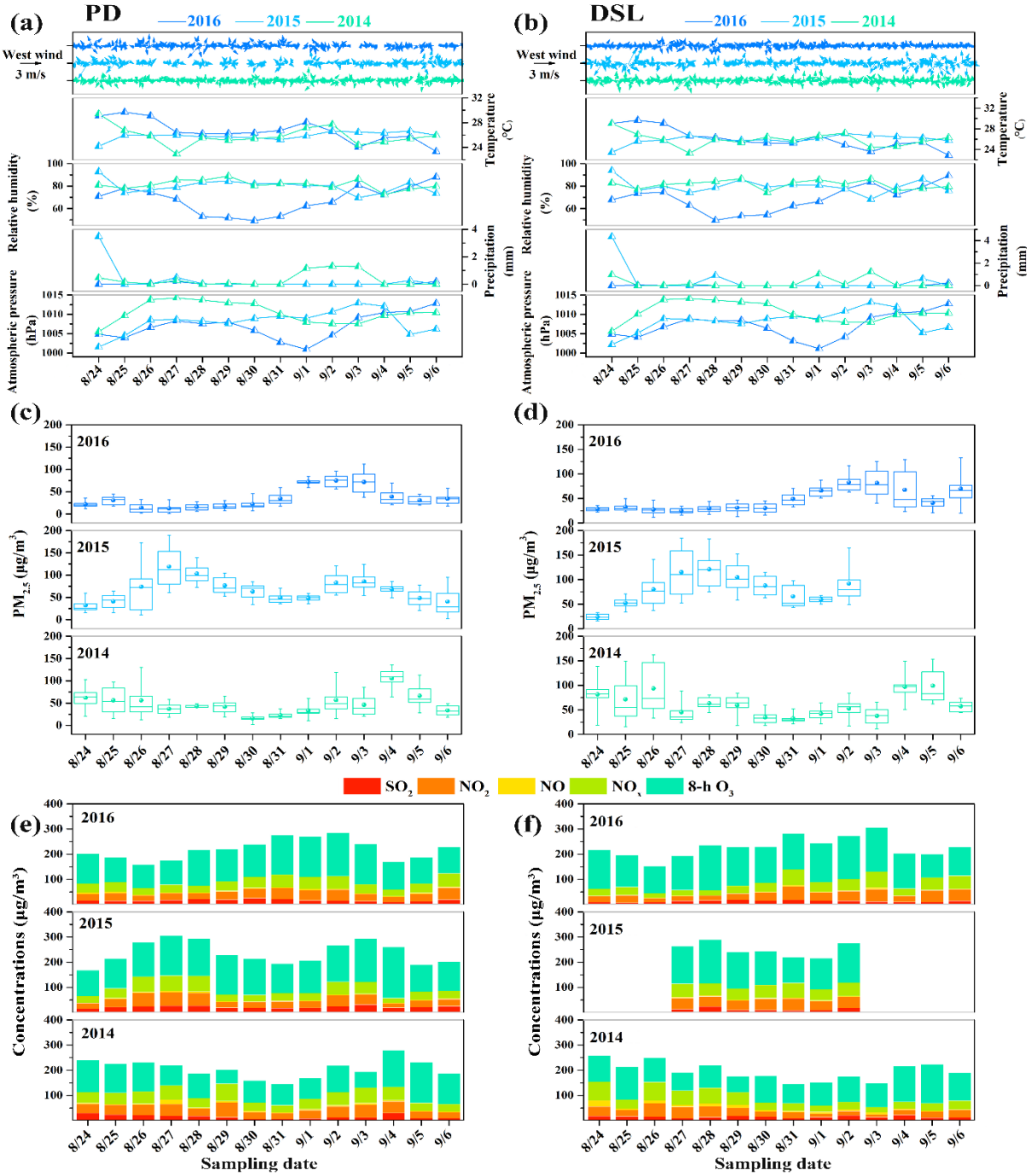
(a)
PD
2016
2015
2014
West wind
3 m/s
Relative humidity (%)
Temperature (℃)
Precipitation (mm)
Atmospheric pressure (hPa)
(b)
DSL
(c)
(d)
PM2.5 (μg/m3)
SO2
NO2
NO
NOx
8-h O3
(e)
(f)
Concentrations (μg/m3)
Sampling date

Fig. 2

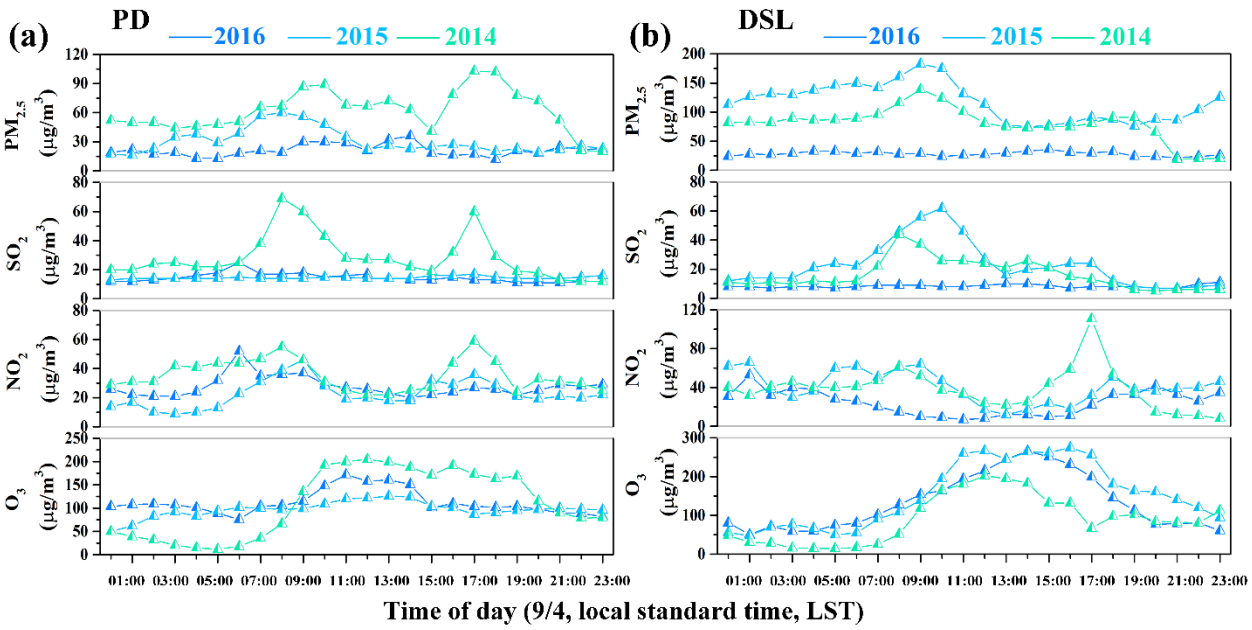
(a)
PD
2016
2015
2014
PM2.5 (μg/m3)
SO2 (μg/m3)
NO2 (μg/m3)
O3 (μg/m3)
(b)
DSL
2016
2015
2014
PM2.5 (μg/m3)
SO2 (μg/m3)
NO2 (μg/m3)
O3 (μg/m3)
01:00 03:00 05:00 07:00 09:00 11:00 13:00 15:00 17:00 19:00 21:00 23:00
Time of day (9/4, local standard time, LST)

473

474 **Fig. 3**

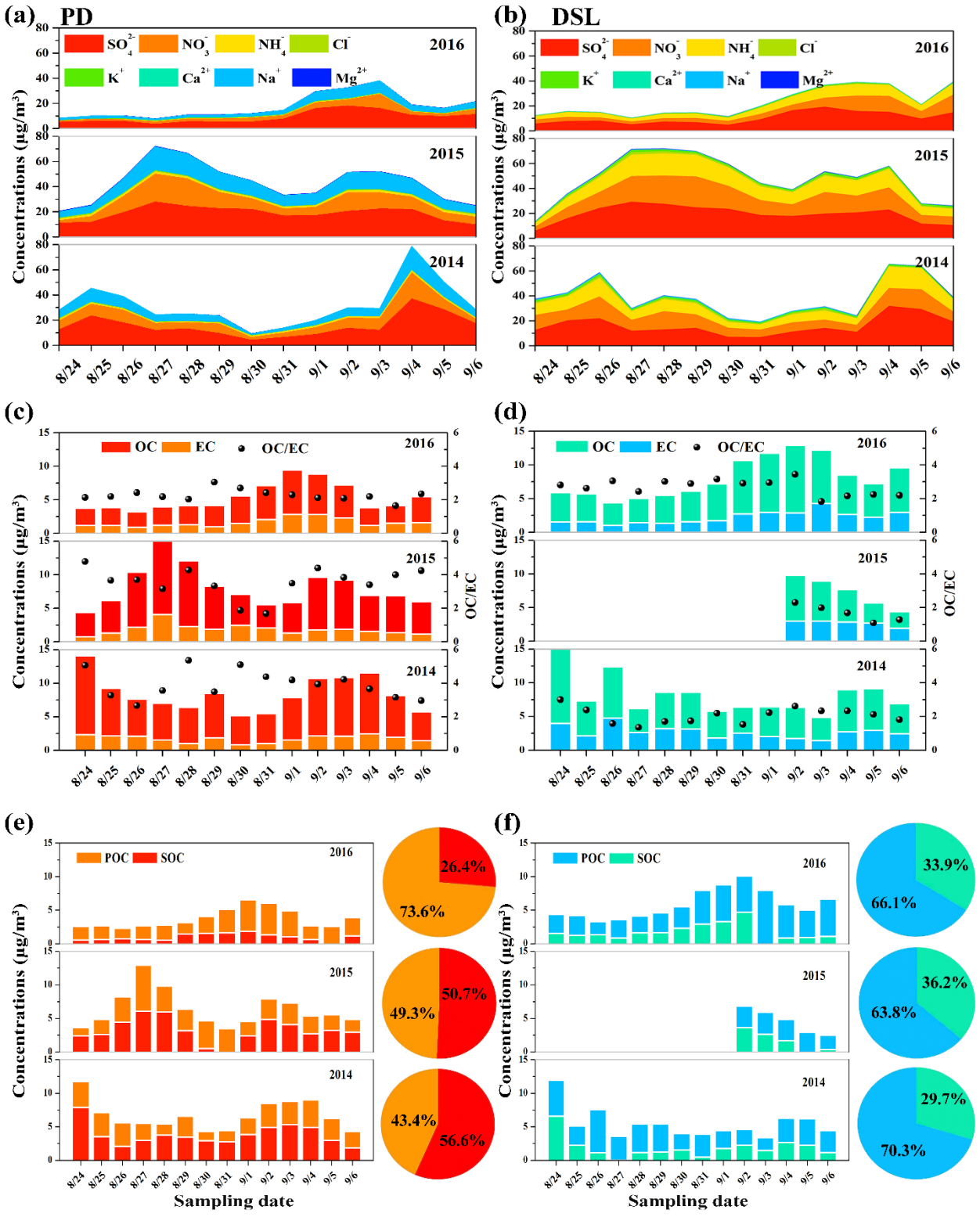
(a) PD
(b) DSL
(c)
(d)
(e)
(f)
Concentrations (μg/m³)
OC/EC
Sampling date
2016
2015
2014
OC
EC
POC
SOC
26.4%
73.6%
50.7%
49.3%
43.4%
56.6%
33.9%
66.1%
36.2%
63.8%
29.7%
70.3%

475

476 **Fig. 4**

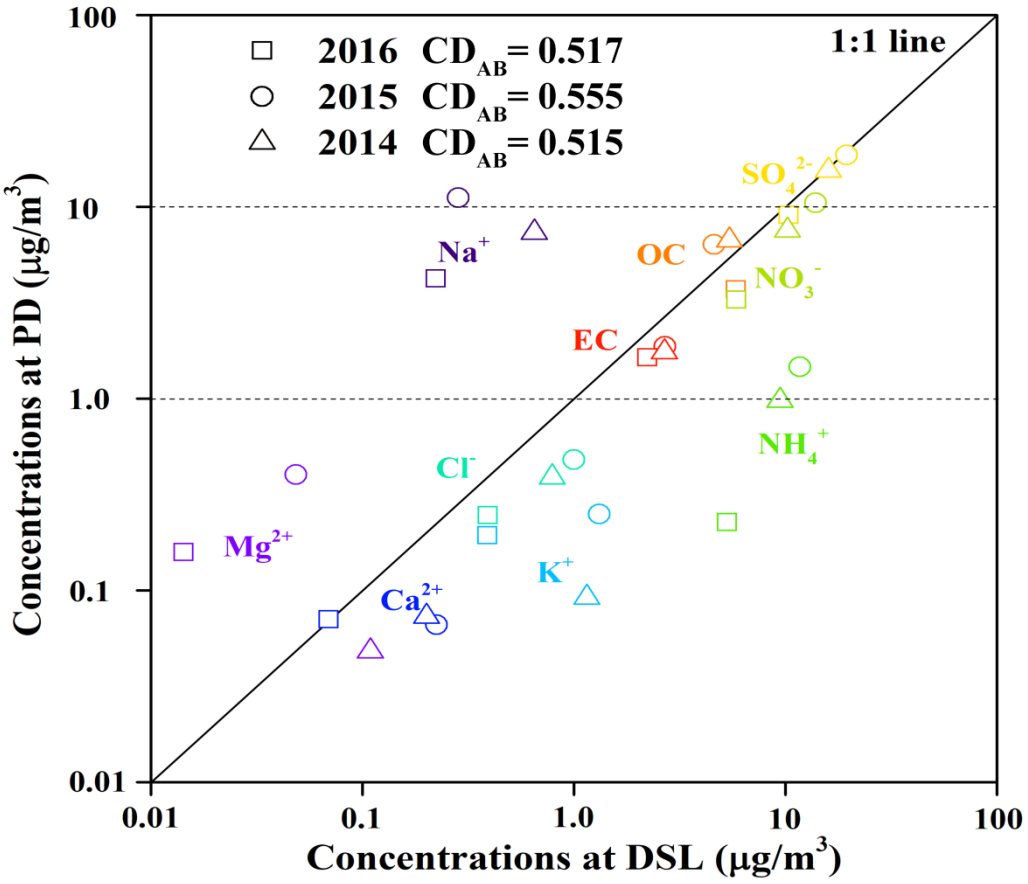
2016 CD$_{AB}$= 0.517
2015 CD$_{AB}$= 0.555
2014 CD$_{AB}$= 0.515
1:1 line
SO$_4^{2-}$
Na$^+$
OC
NO$_3^-$
EC
NH$_4^+$
Cl$^-$
Mg^{2+}
K$^+$
Ca^{2+}
Concentrations at PD (μg/m^3)
Concentrations at DSL (μg/m^3)
100
10
1.0
0.1
0.01
0.01
0.1
1.0
10
100

477

478 **Fig. 5**

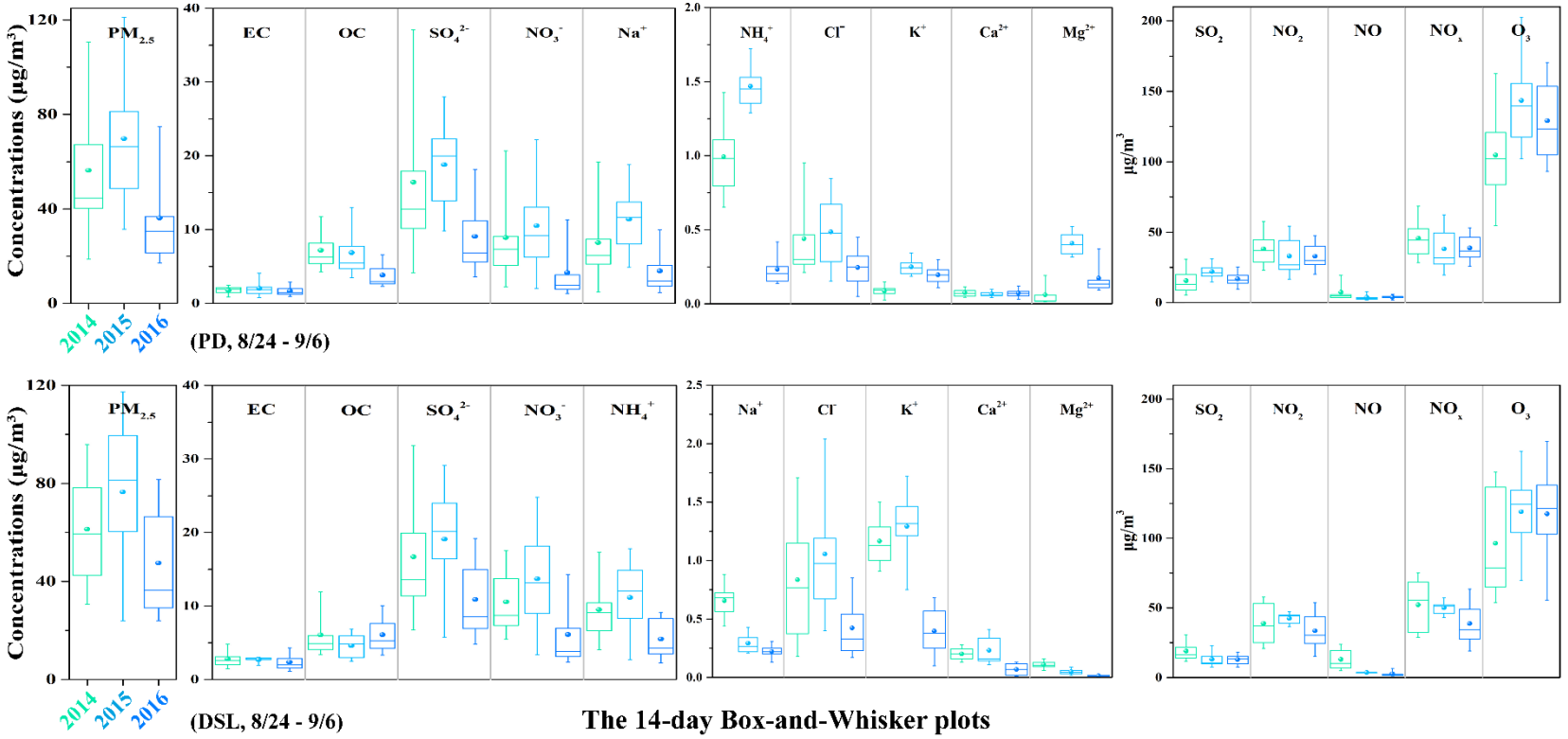
Concentrations (μg/m³)
PM2.5
EC
OC
SO4 2-
NO3-
Na+
NH4+
Cl-
K+
Ca2+
Mg2+
SO2
NO2
NO
NOx
O3
μg/m3
2014
2015
2016
(PD, 8/24 - 9/6)
(DSL, 8/24 - 9/6)
The 14-day Box-and-Whisker plots

Fig. 6

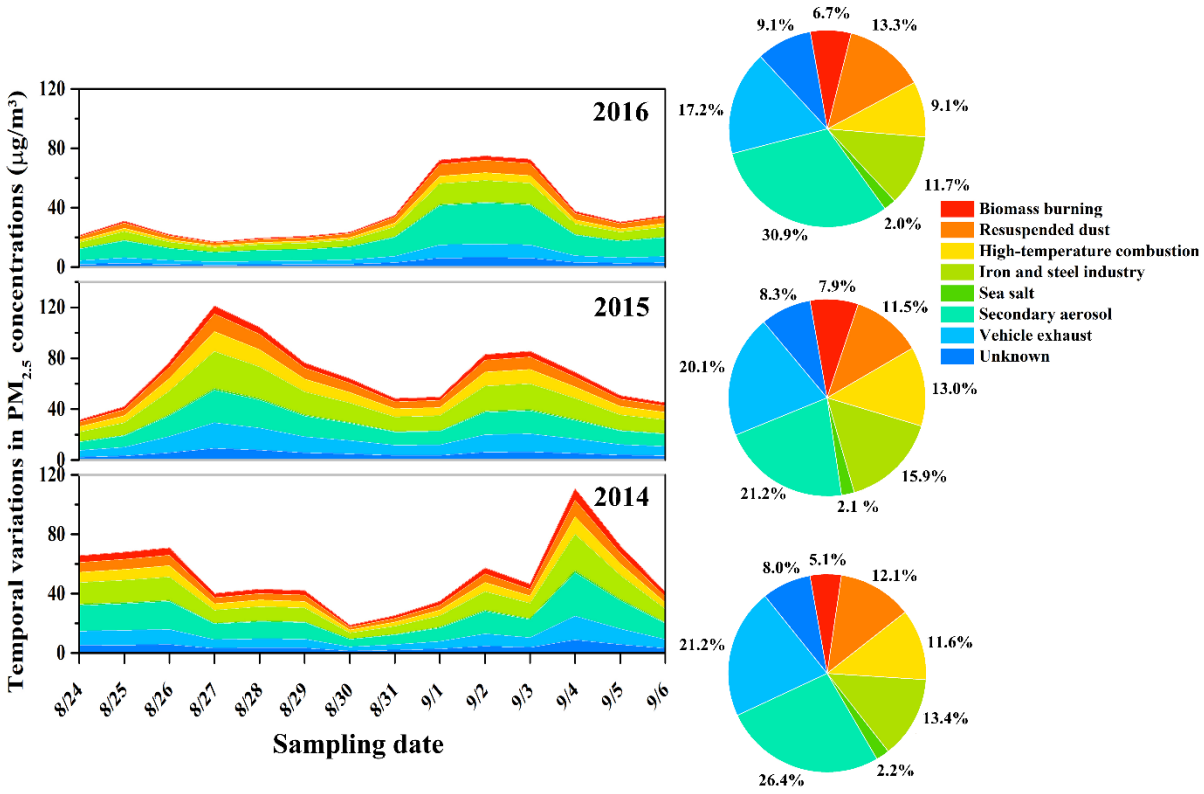
2016
2015
2014
Temporal variations in PM2.5 concentrations (μg/m³)
Sampling date
8/24
8/25
8/26
8/27
8/28
8/29
8/30
8/31
9/1
9/2
9/3
9/4
9/5
9/6
9.1%
6.7%
13.3%
17.2%
9.1%
11.7%
30.9%
2.0%
8.3%
7.9%
11.5%
20.1%
13.0%
15.9%
21.2%
2.1 %
8.0%
5.1%
12.1%
21.2%
11.6%
13.4%
26.4%
2.2%
Biomass burning
Resuspended dust
High-temperature combustion
Iron and steel industry
Sea salt
Secondary aerosol
Vehicle exhaust
Unknown

481

482 **Fig. 7**

Figure 1

Click here to download high resolution image

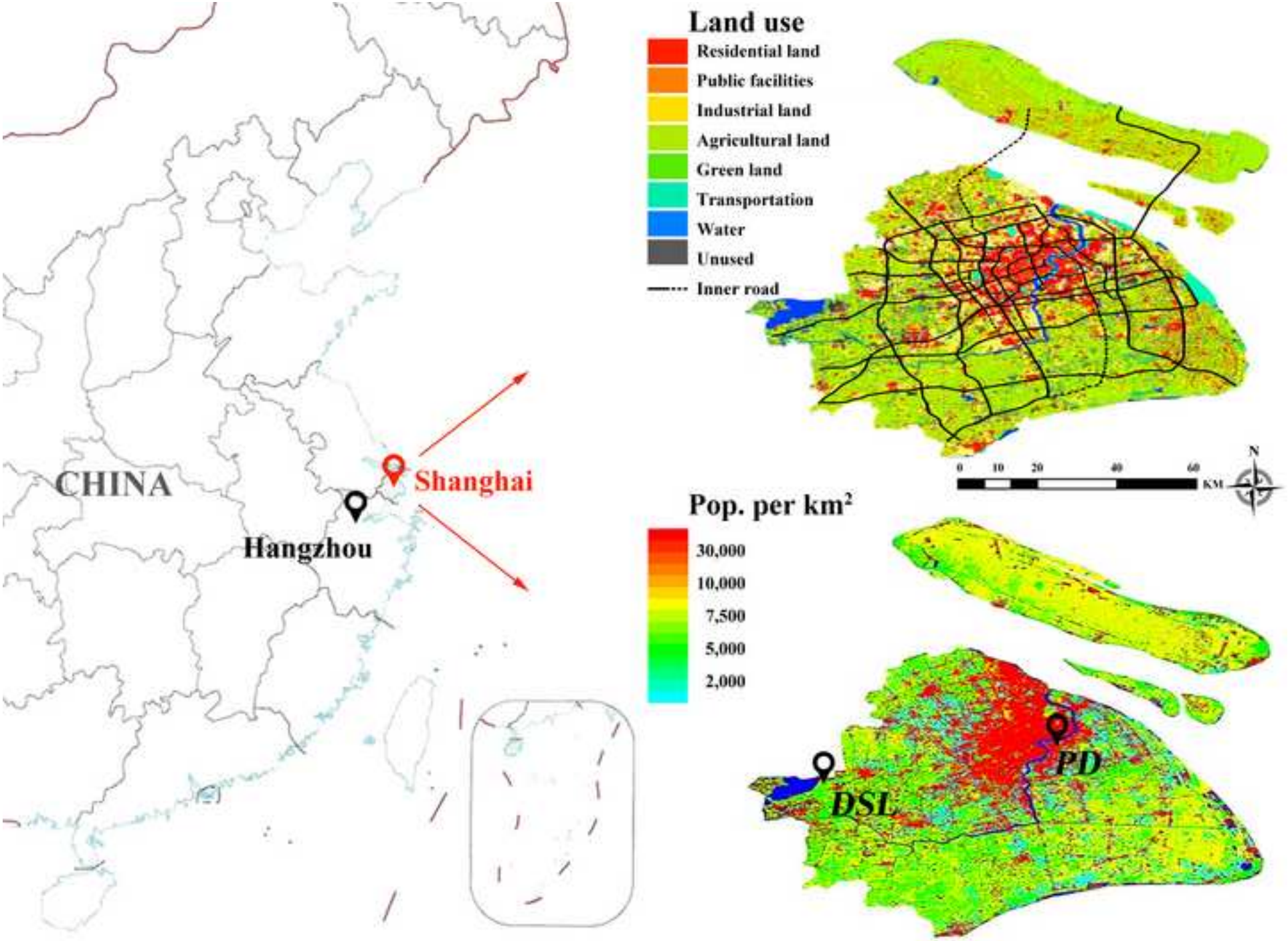

Figure 2

Click here to download high resolution image

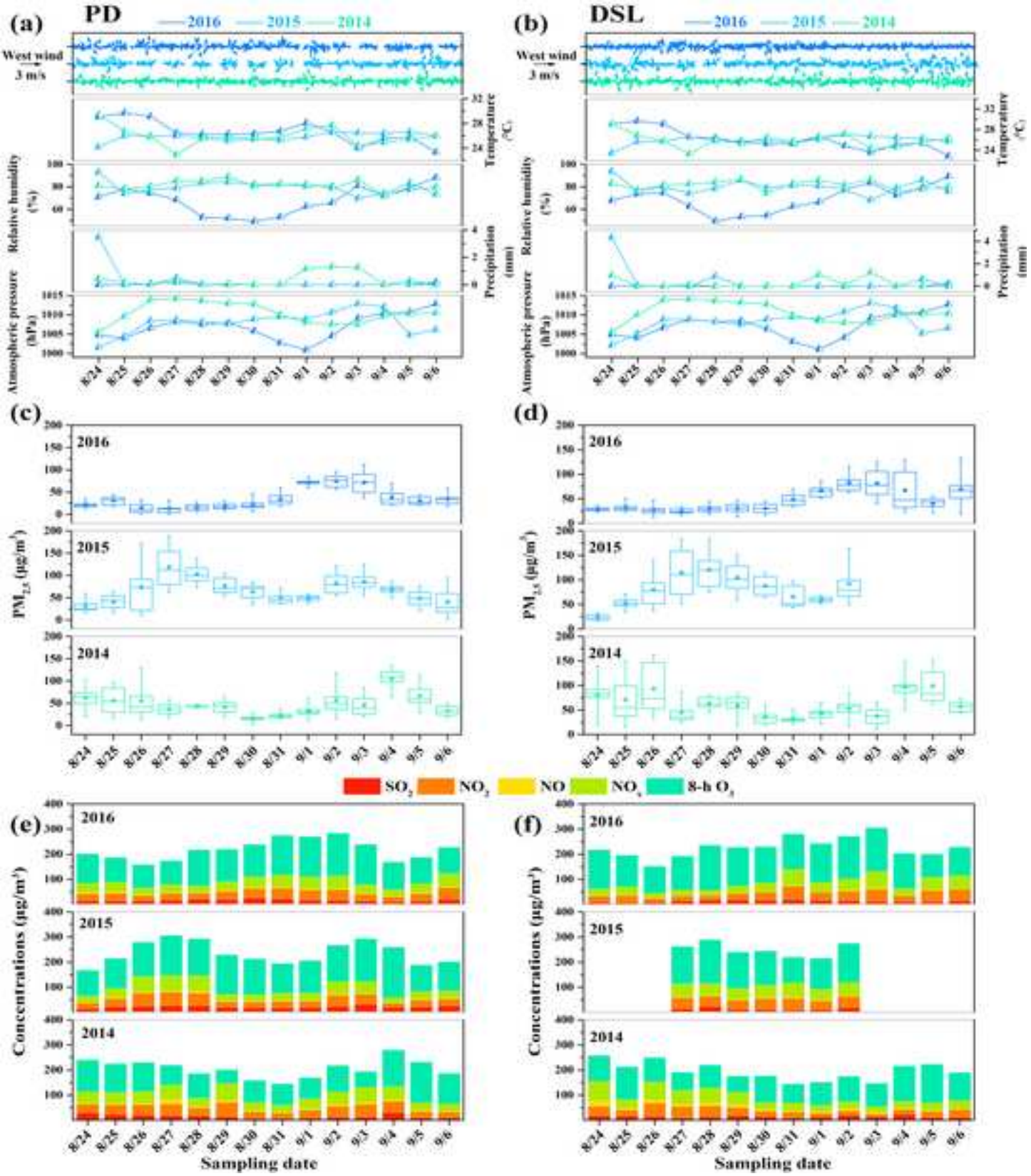

Figure 3

Click here to download high resolution image

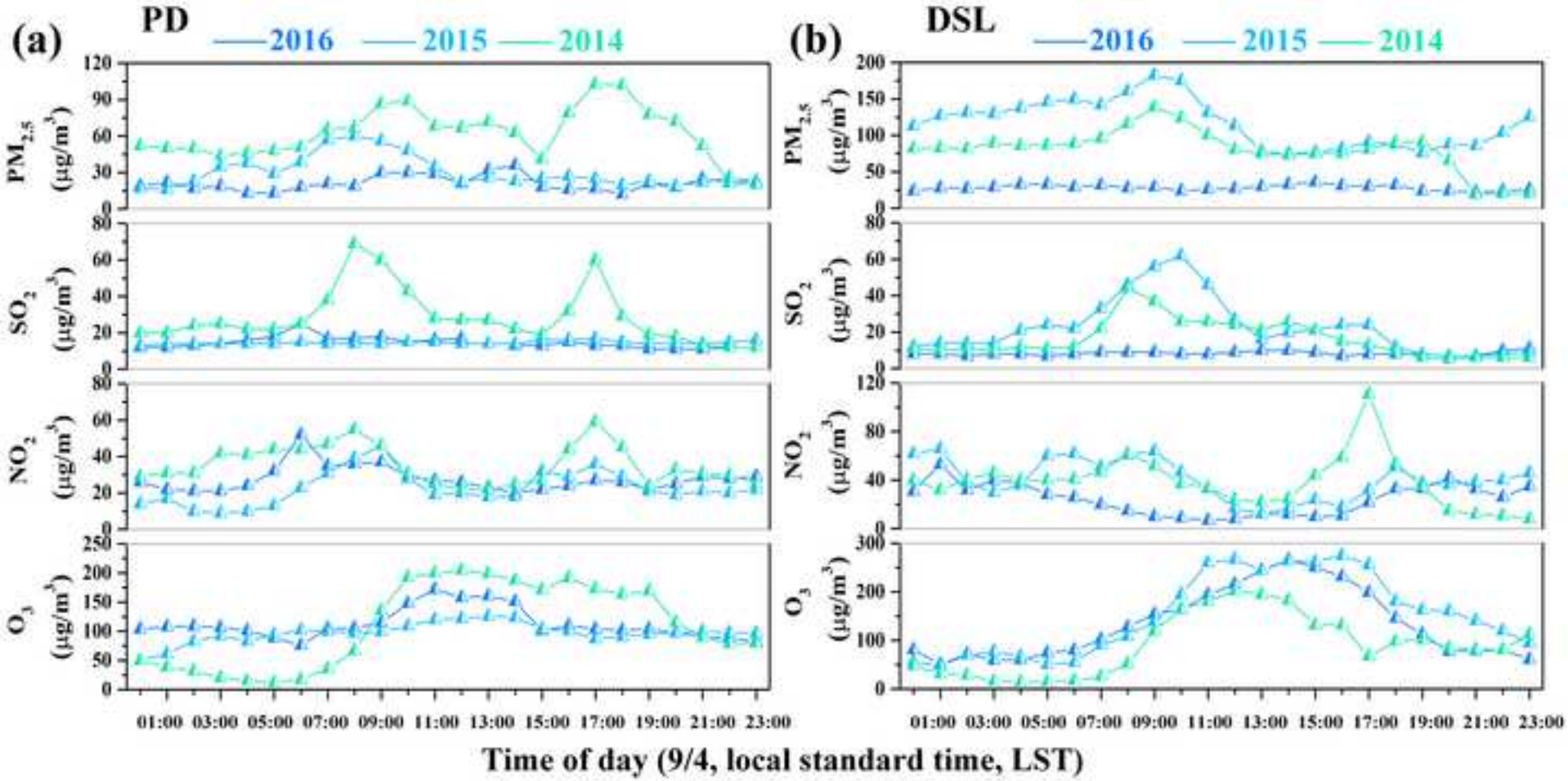

Figure 4

Click here to download high resolution image

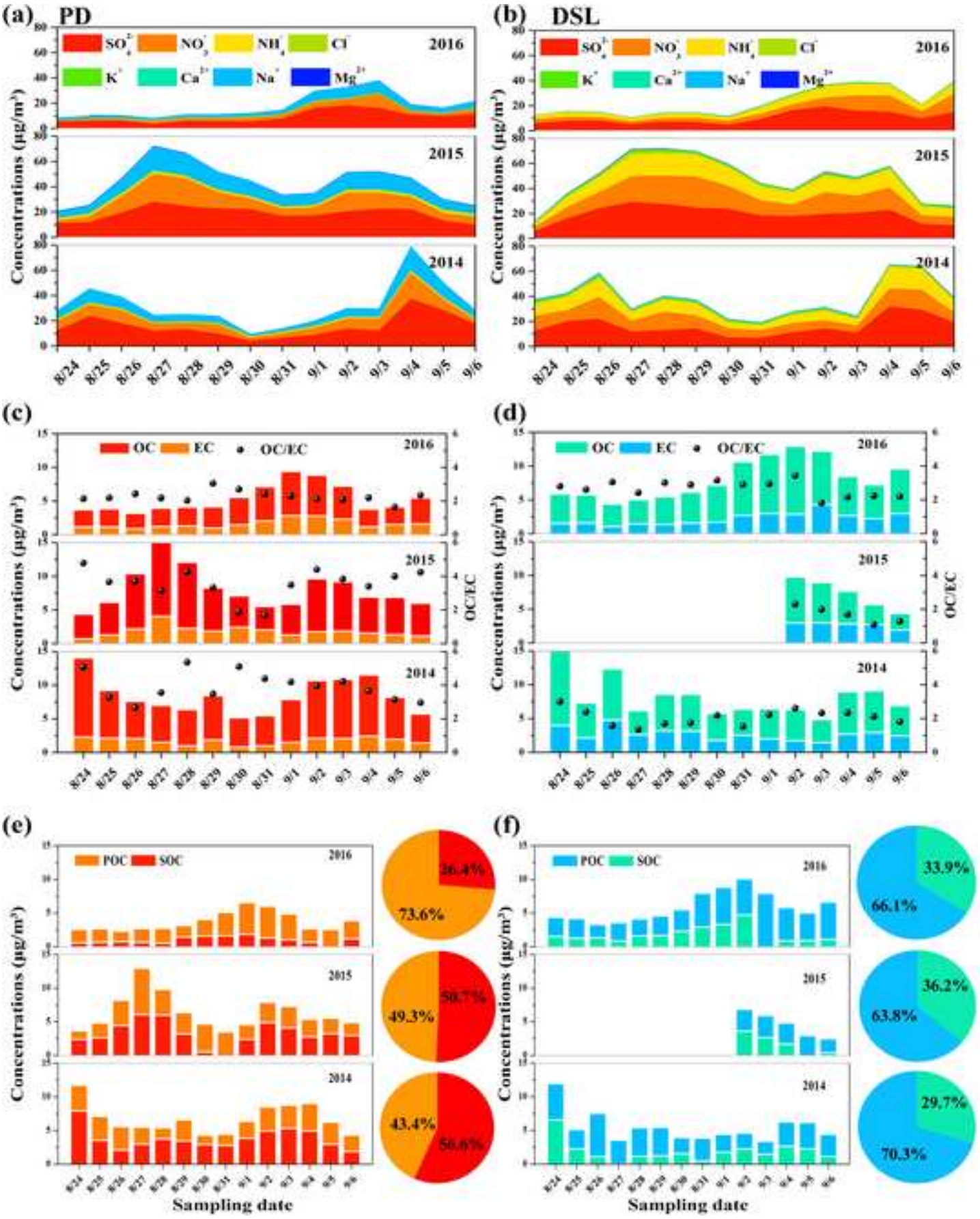

Figure 5

Click here to download high resolution image

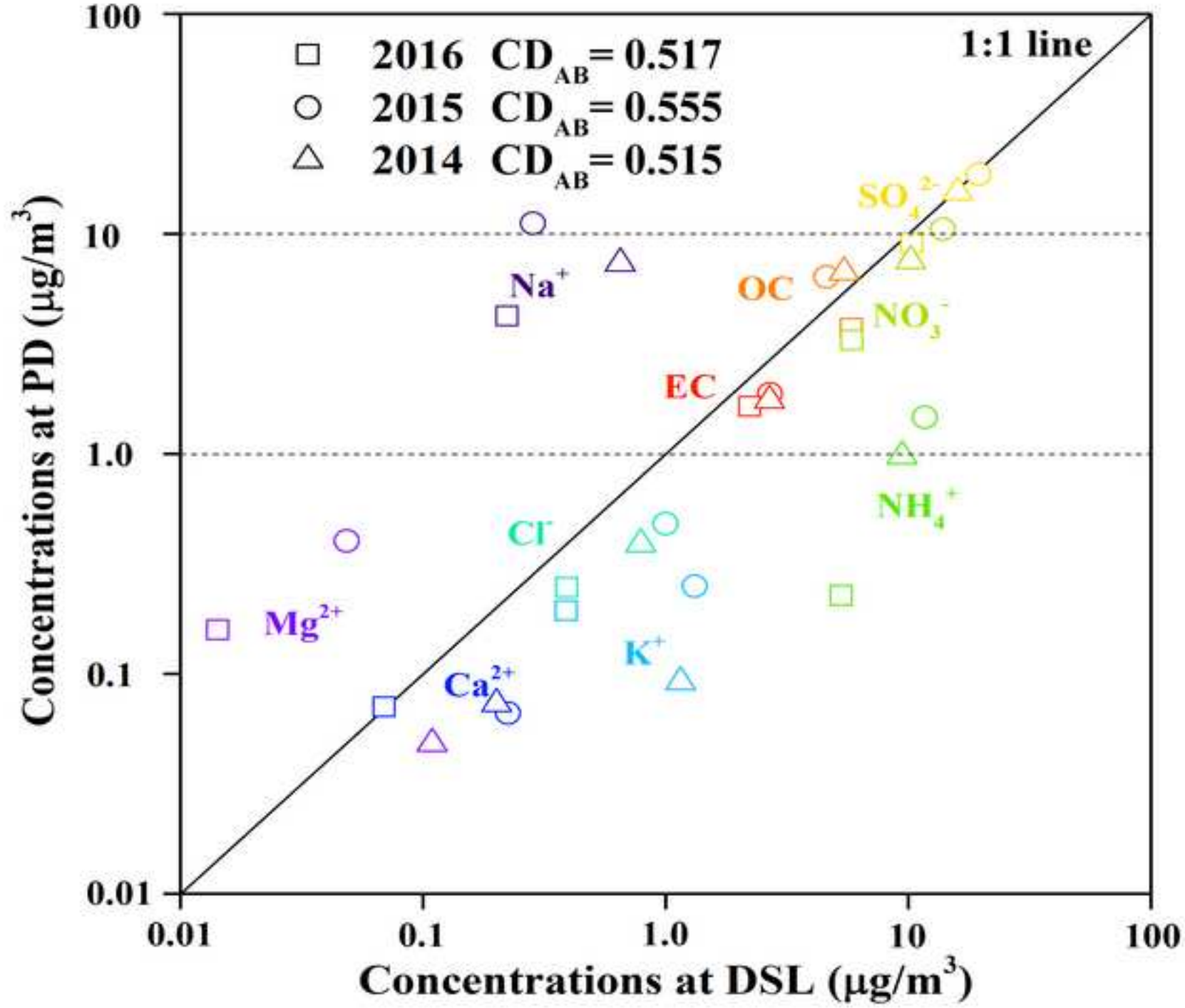

Figure 6

Click here to download high resolution image

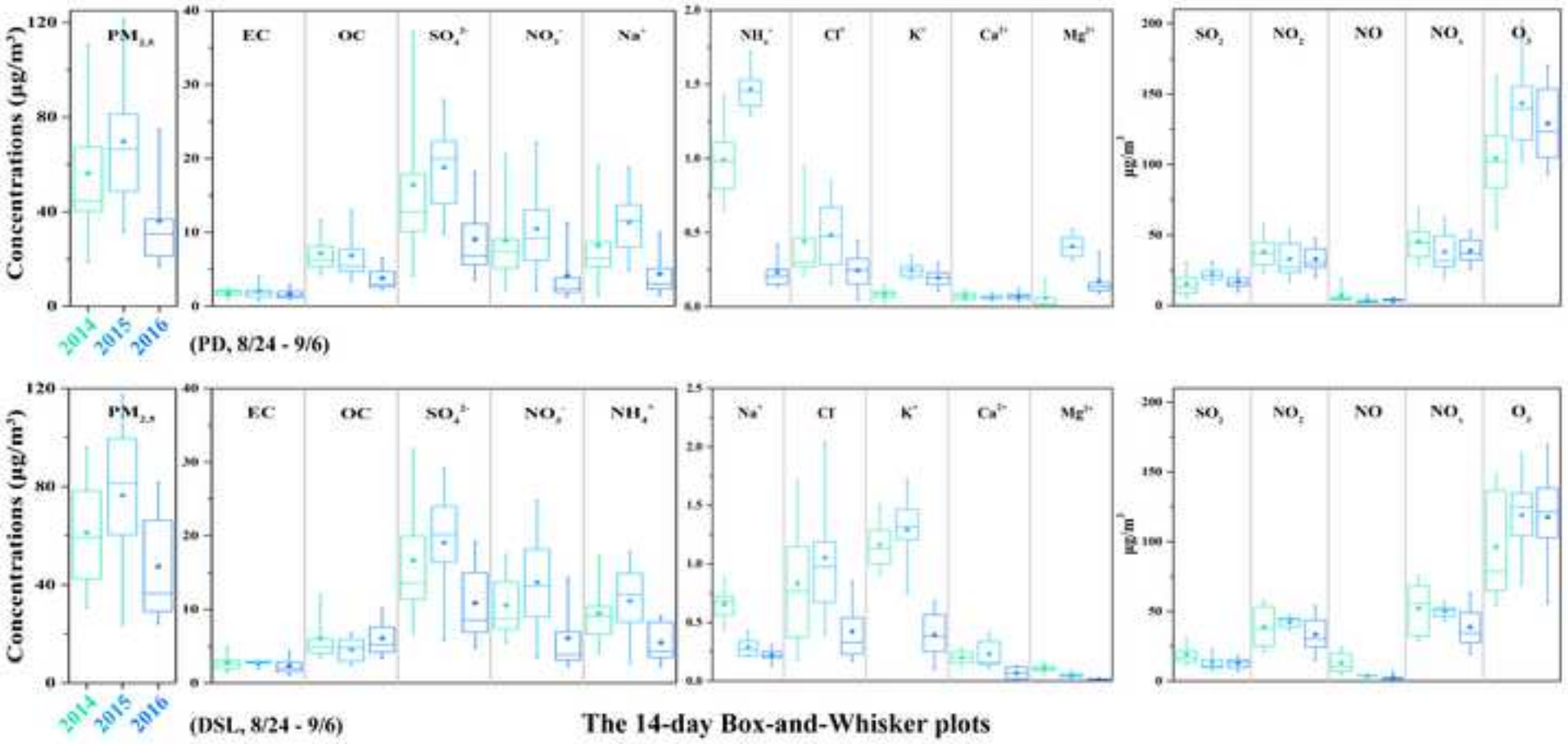

Figure 7

Click here to download high resolution image

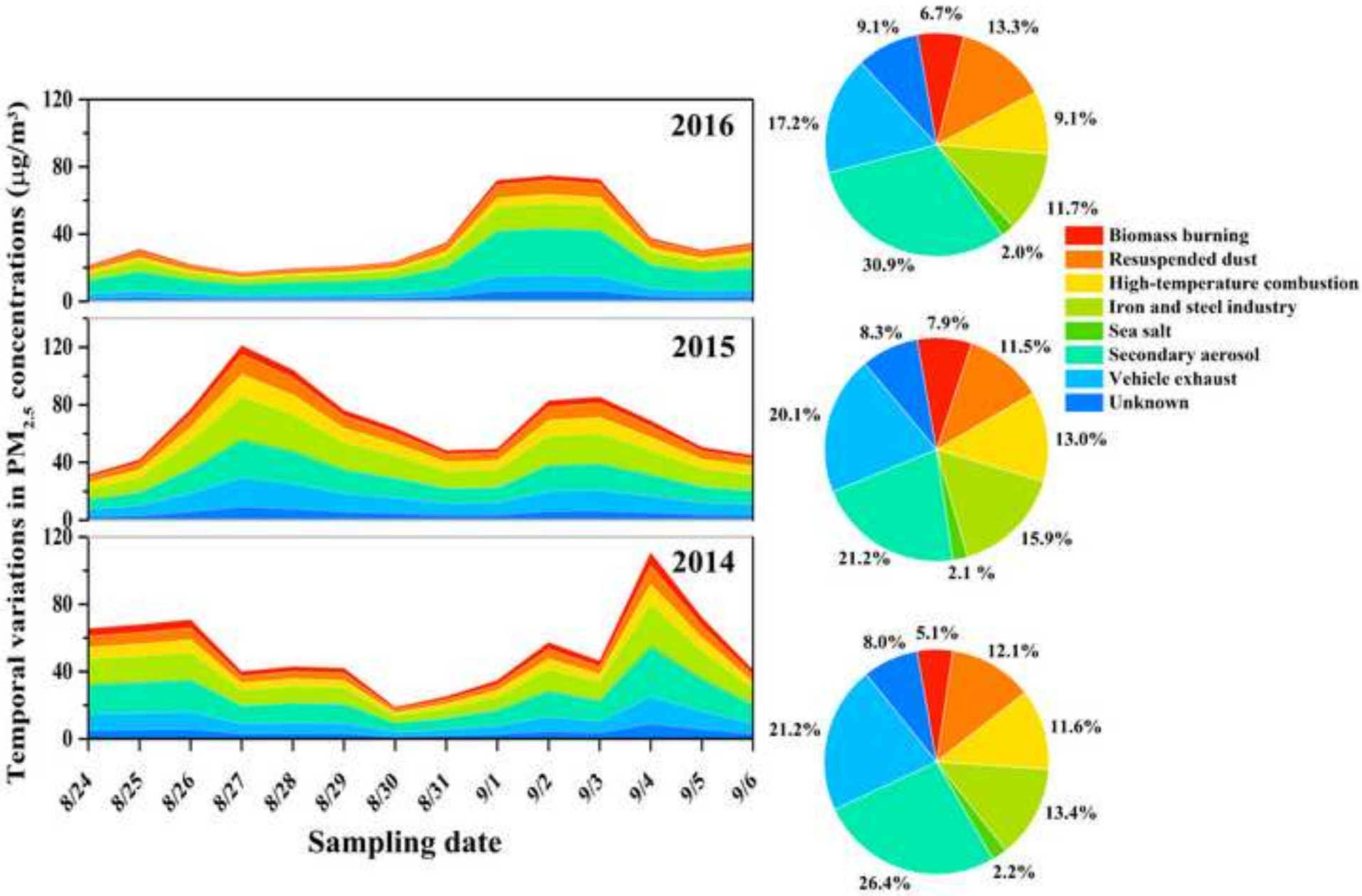

Supplementary material for on-line publication only

Click here to download Supplementary material for on-line publication only: Supplementary Information_STE.docx